Earth and Planetary Science Letters 362 (2013) 6–19

Contents lists available at SciVerse ScienceDirect

Earth and Planetary Science Letters

journal homepage: www.elsevier.com/locate/epsl

Segmentation of the Hellenides recorded by Pliocene initiation of clockwise block rotation in Central Greece

Kyle E. Bradley [a,*], Emmanuel Vassilakis [b], Aleksandra Hosa [a,1], Benjamin P. Weiss [a]

[a] Department of Earth, Atmospheric, and Planetary Sciences, Massachusetts Institute of Technology, Cambridge, MA 02139, USA
[b] Department of Geology, University of Athens, Panepistimioupolis, Zografou, 15784 Athens, Greece

ARTICLE INFO

Article history:
Received 11 July 2012
Received in revised form
14 November 2012
Accepted 19 November 2012
Editor: L. Stixrude

Keywords:
Aegean
paleomagnetism
rotation
subduction
tectonics

ABSTRACT

New paleomagnetic data from Early Miocene to Pliocene terrestrial sedimentary and volcanic rocks in Central Greece constrain the history of vertical-axis rotation along the central part of the western limb of the Aegean arc. The present-day pattern of rapid block rotation within a broad zone of distributed deformation linking the right-lateral North Anatolian and Kephalonia continental transform faults initiated after Early Pliocene time, resulting in a uniform clockwise rotation of $24.3 \pm 6.5^\circ$ over a region >250 km long and >150 km wide encompassing Central Greece and the western Cycladic archipelago. Because the published paleomagnetic dataset requires clockwise rotations of $>50^\circ$ in Western Greece after $\sim$17 Ma, while our measurements resolve no vertical-axis rotation of Central Greece between $\sim$15 Ma and post-Early Pliocene time, a large part of the clockwise rotation of Western Greece must have occurred during the main period of contraction within the external thrust belt of the Ionian Zone between $\sim$17 and $\sim$15 Ma. Pliocene initiation of rapid clockwise rotation in Central and Western Greece reflects the development of the North Anatolia–Kephalonia Fault system within the previously extended Aegean Sea region, possibly in response to entry of dense oceanic lithosphere of the Ionian Sea into the Hellenic subduction zone and consequent accelerated slab rollback. The development of the Aegean geometric arc therefore occurred in two short-duration pulses characterized by rapid rotation and strong regional deformation.

1. Introduction

Slab retreat resulting from high rates of buoyancy-driven subduction within a broader context of slow plate convergence has been proposed as the primary cause of orogenic curvature in the circum-Mediterranean region (Faccenna et al., 2004; McKenzie, 1978; Rosenbaum and Lister, 2004; Royden, 1993; Royden and Husson, 2009). The expanding interior regions of these arcuate mountain belts (Fig. 1) are commonly occupied by crustal blocks that were laterally displaced from adjacent regions of continent–continent collision along lithospheric-scale strike slip faults (Ustaszewski et al., 2008; van Hinsbergen et al., 2008). Paleogeography therefore appears to largely dictate the style and tempo of crustal deformation along complex collisional boundaries.

In the case of the Aegean region, the long-term tectonic development of the Hellenic arc has been linked to the paleogeography of the northward-subducting Nubian–Arabian lithospheric plate (Jolivet and Brun, 2010; Papanikolaou and Royden, 2007; Royden and Papanikolaou, 2011). In this model, entry of very negatively-buoyant Ionian Sea oceanic lithosphere into the Hellenic trench increased the rate of subduction south of the island of Kephalonia, resulting in rapid trench retreat and fragmentation of the overriding plate. Coincident with crustal extension in the Aegean Sea, Anatolia moved westward away from the Arabian–Eurasian continental collision zone along the dextral-sense North Anatolian Shear Zone (Şengör et al., 2005). This region therefore contains each of the major tectonic components that characterize the small circum-Mediterranean orogens and has been an incubator for tectonic and geodynamic concepts relating subduction dynamics to continental tectonics.

The Hellenic geometric arc (in contrast with the active volcanic arc) is defined by a topographic and bathymetric high that extends over a distance of $\sim$1500 km from northern Albania to western Anatolia, paralleling the trend of accreted crustal tracts and the Hellenic bathymetric trench (Fig. 1, dashed box). Long-term, buoyancy-driven rollback of a continuous Nubian lithospheric slab away from Europe is commonly inferred from the geological record

* Corresponding author. Now at: Earth Observatory of Singapore, Nanyang Technological University, Block N2-01a-15, 50 Nanyang Avenue, Singapore 639798, Singapore. Tel.: +65 65922494.
E-mail address: kbradley@ntu.edu.sg (K.E. Bradley).
[1] Now at: School of Geosciences, University of Edinburgh, Edinburgh EH9 3JW, UK.

0012-821X/$ - see front matter © 2012 Elsevier B.V. All rights reserved.
http://dx.doi.org/10.1016/j.epsl.2012.11.043

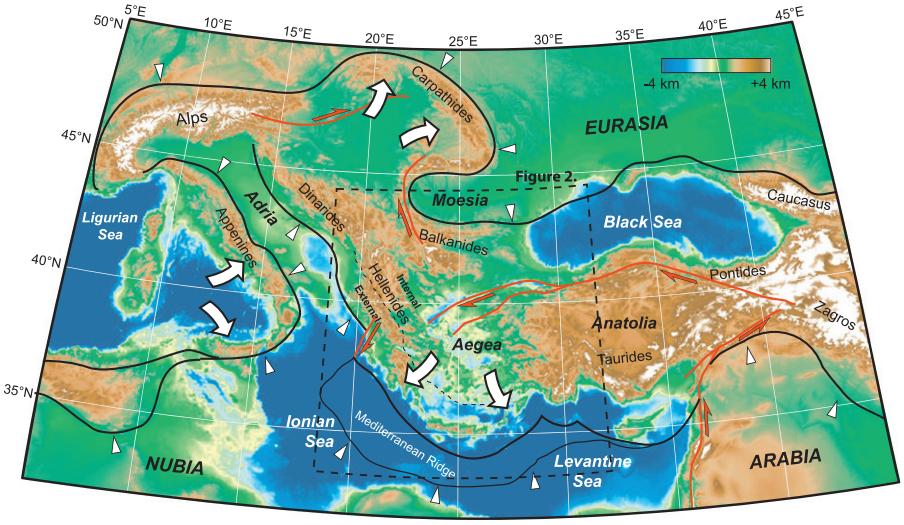

Fig. 1. Simplified tectonic map of the Eastern Mediterranean region showing the arcuate form of the orogenic belts that decorate the southern Eurasian margin. Curved arrows indicate the apparent sense of rotation along the frontal thrust belt that accompanied geometric arc formation. Small wedges show the sense of underthrusting along crustal deformation fronts (black lines). Topography and bathymetry are from the ETOPO-1 dataset (Amante et al., 2009). Dashed box indicates the location of Fig. 2.

of underthrusting and subsequent exhumation of rocks exposed in the Aegean upper plate (Faccenna et al., 2004; Jolivet and Brun, 2010; van Hinsbergen et al., 2005b). While the most internal tectonic units were attached to stable Europe for at least the last 35 million years (Myr) and therefore rotated slowly clockwise (Besse and Courtillot, 2002), the accreted crust of the External Hellenides thrust belt moved northward with the Nubian plate without significant rotation and was progressively accreted to the southern margin of the Eurasian plate (Jolivet and Brun, 2010). The record of displacement and rotation of these rocks since Cretaceous time is therefore central to understanding the complexities of this long-lived intra-plate convergence zone.

Due to the geocentric axial dipolar nature of the time-averaged geomagnetic field, the direction of paleomagnetic remanence preserved in sedimentary and igneous rocks provides a time-integrated, spatially-distributed record of vertical-axis rotation and latitudinal translation of Earth's crust that allows geometric reconstruction of regions of complex crustal deformation through time (Weil and Sussman, 2004). These reconstructions provide an essential element of time control to geodynamical models that seek to explain the tectonic evolution of subduction-bounded collisional belts in terms of fundamental physical processes (Cifelli et al., 2008; Dupont-Nivet et al., 2005; Kissel, 2003; Papanikolaou and Royden, 2007; Platt, 2007). Because the primary causes of vertical-axis rotation are global plate motion, bending of collisional belts into continuous or segmented oroclines, and rotation of internally rigid blocks within diffuse transcurrent fault systems, paleomagnetic data are uniquely suited for unraveling the record of crustal deformation in a variety of overriding plate settings.

Paleomagnetic declinations preserved within imbricated Cretaceous through Miocene sedimentary rocks exposed within the External Hellenides of western mainland Greece (Fig. 2) exhibit a consistent pattern of large-magnitude, clockwise-sense vertical-axis rotation (Broadley et al., 2006; Horner and Freeman, 1983; Kissel et al., 1986a; Kissel and Laj, 1988; Mauritsch et al., 1996; Speranza et al., 1992; van Hinsbergen et al., 2005a, 2006). This rotation locally exceeds 50° and is thought to reflect extensional decoupling of the frontal thrust belt from the stable, non-rotating back-arc region (Fig. 2) during accelerated rollback of the subducting African lithospheric slab away from the stable Eurasian plate since Middle Miocene time (Brun and Sokoutis, 2007; Jolivet and Brun, 2010; Ring et al., 2010; Royden and Papanikolaou, 2011; van Hinsbergen et al., 2005a, 2008). Further evidence for large-scale rotation in the overriding plate arising from retreat of the Hellenic slab comes from Western Anatolia (Fig. 2), where counter-clockwise vertical-axis rotations were accommodated by crustal extension within the Menderes metamorphic complex (van Hinsbergen et al., 2010).

At present, the northern Aegean Sea and the Greek mainland are transected by a complex system of strike-slip and normal faults that accommodate rapid westward-to-southwestward motion of western Anatolia and the south Aegean with respect to Eurasia (Angelier et al., 1982; Dewey and Şengör, 1979; Floyd et al., 2010; McClusky et al., 2000; Reilinger et al., 2010, 2006). Right-lateral slip is transferred from the North Anatolian Fault system through the North Aegean Trough (Le Pichon, 2003; Papanikolaou et al., 2002), into the extensional province of Central Greece (Mckenzie and Jackson, 1983; Roberts and Jackson, 1991), and finally through the right-lateral Kephalonia and Achaia faults into the rapidly retreating, northeast-vergent Hellenic subduction zone (Vassilakis et al., 2011). This diffuse crustal shear zone is characterized by rapid (~2–4°/Myr) clockwise rotations as inferred from high-density geodetic data (Floyd et al., 2010; Nyst and Thatcher, 2004). Paleomagnetic data from Late Miocene and Pliocene sediments exposed on the Ionian Islands show that the modern pattern of rapid clockwise rotation initiated in this region during Pliocene time, coincident with reactivation of thrusting along the western edge of the Ionian Zone (Duermeijer et al., 1999; Kissel et al., 1986b; Kondopoulou and Caputo, 1997; Laj et al., 1982; van Hinsbergen et al., 2005a).

The net Neogene clockwise rotation at a given locality in Western Greece is therefore primarily the sum of two rotations—a large-scale rotation related to arc formation and a more localized, transform-related rotation that accentuated the previously established geometric arc. Unfortunately, the spatial distribution of Middle Miocene to Pleistocene sediments and volcanics is generally insufficient to constrain the last 15 Myr of rotation at a single locality. In the External Hellenides thrust belt, Cretaceous through Early/Middle Miocene sediments are abundant; however, the unconformably overlying sedimentary sequences are primarily Plio-Pleistocene in age. In the Internal

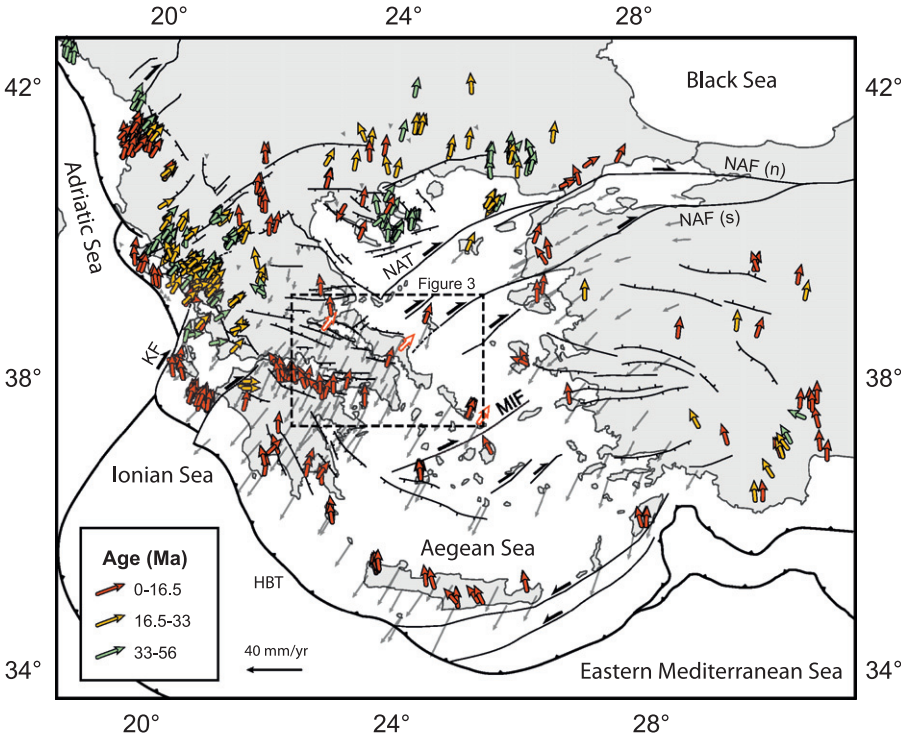

Fig. 2. Paleomagnetic, geodetic, and structural framework for the Aegean region. Colored arrows indicate published paleomagnetic site- and locality-mean declinations, categorized by the inferred age of magnetization (references are presented in Supplementary Text S.1). Open arrows in Central Greece indicate declinations that we consider unreliable (see main text). Gray arrows are GPS velocity vectors from Floyd et al. (2010), plotted relative to stable Europe, with some data in Central Greece omitted for clarity. Late Cenozoic brittle faults are generalized from Taymaz et al. (1991), Goldsworthy et al. (2002), and Jolivet and Brun (2010). KF: Kephalonia Fault; NAT: North Aegean Trough; NAF (n,s): North Anatolian Fault (northern strand, southern strand); MIF: Mirthes–Ikaria Fault; HBT: Hellenic bathymetric trench. (For interpretation of the references to color in this figure legend, the reader is referred to the web version of this article.)

Hellenides, and particularly the northern Pelagonian Zone, Oligo-Miocene sediments are restricted to the Mesohellenic Trough and the Neogene terrestrial basins are of latest Miocene and Pliocene ages. The result of this incomplete data coverage is a persistent uncertainty in the duration and distribution of crustal rotation that transfers into uncertainties in the evolution of causative geodynamic forces in the region.

Right-lateral shearing along the North Anatolian and Kephalonia–Achaia continental transform fault systems is taken up by nearly equal components of northeast (NE)–southwest (SW) directed shortening and northwest (NW)–southeast (SE) directed dilation, and extensional basins are therefore not commonly developed or subaerially exposed in these regions (Floyd et al., 2010). In contrast, the intermediate region of Central Greece is deforming solely by north (N)–south (S) directed extension accompanied by rapid vertical-axis block rotation in a clockwise sense (Floyd et al., 2010; Mckenzie and Jackson, 1983). This largely subaerial extensional province preserves an abundance of well-exposed, fault-delimited sedimentary sequences of Early Miocene through Plio-Pleistocene age (Papanikolaou and Royden, 2007), and has been the focus of a number of studies that have attempted to relate the spatial pattern and rate of vertical-axis block rotations to the rheology of the continental crust during distributed shearing (McKenzie and Jackson, 1983; Taymaz et al., 1991; Goldsworthy et al., 2002).

In this study, we present new paleomagnetic measurements from Early Miocene to Pliocene terrestrial basins and associated volcanic units in Central Greece, which directly constrain the history of vertical-axis rotation over the last ~15 Myr. The sampled region has the appropriate geographic position and stratigraphic record to constrain the large-scale rotation of the Hellenides and the subsequent development of the trans-Aegean continental transform system.

2. Paleomagnetic methods

We sampled five Neogene sedimentary basins and four igneous units in Central Greece for paleomagnetic analysis (Fig. 3). In this study, the term "site" refers to a single sedimentary bed or continuous outcrop of volcanic rock that is expected to record the instantaneous (averaged over <1000 yr) geomagnetic field direction, while "locality" refers to similarly aged rocks within a small geographic region (<10 km radius). We collected 2.54 cm diameter cores using a diamond-bit gasoline-powered drill, with spatial orientation obtained by both magnetic and sun compasses. All samples were cut into 1.3 cm tall cylindrical specimens using a water-cooled saw with nonmagnetic blades and were stored in a shielded room (DC field <200 nT) for one month prior to analysis to allow decay of viscous remanent magnetizations. Between five and 20 cores were collected from each site, each yielding one to three oriented specimens. We measured paleomagnetic remanence using a 2G Superconducting Rock Magnetometer (SRM) 755 with a sensitivity of 1×10^{-9} Am^2 in the MIT Paleomagnetism Laboratory equipped with an automatic sample changer and in-line rock magnetism instruments (Kirschvink et al., 2008). Specimens with a very low-intensity natural remanent magnetization (NRM) ($<1\times10^{-5}$ A/m) were discarded without further analysis due to the low probability of isolating a characteristic remanent magnetization (ChRM). While selected specimens were subjected to alternating field (AF) demagnetization up to maximum applied fields of 85 mT, we thermally demagnetized most specimens in a magnetically shielded ASC scientific oven with an ambient field intensity of <10 nT. We processed the resulting demagnetization data using standard paleomagnetic software (Cogné, 2003; Jones, 2002; Tauxe et al., 2009). We calculated linear components from demagnetization trends using the least-squares method of Kirschvink (1980).

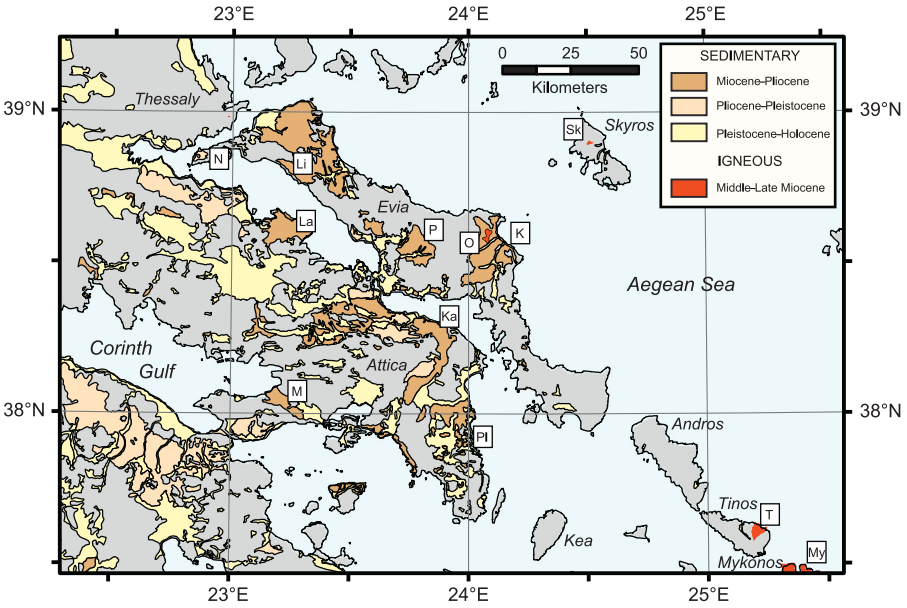

Fig. 3. Simplified geological map showing the distribution of igneous rocks and Miocene–Pliocene, Pliocene–Pleistocene, and Pleistocene–Holocene surficial deposits, and igneous rocks in Central Greece. Localities discussed in the text are indicated by boxed letters (key is given in Fig. 4).

Table 1
Locality mean directions presented in this study, calculated using Fisher averaging of site-mean directions. The resulting grand mean direction for Central Greece is indicated in bold.

Locality	*N*	*D* (deg.)	Δ*D* (deg.)	*I* (deg.)	Δ*I*, α_{95} (deg.)	*k*	*R*	Lat (°N)	Lon (°E)
Markopoulo	7	27.4	9.6	55.3	5.4	122.7	5.977	38.30	23.89
Larymna	8	35.4	12.0	51.4	7.4	56.2	7.876	38.61	23.24
Kymi	24	23.6	8.7	56.8	4.5	39.8	23.423	38.58	24.14
Limni	17	25.4	9.8	54.2	5.7	39.9	16.600	38.78	23.31
Palioura	8	23.4	8.4	56.3	4.6	144.1	7.951	38.60	23.80
Oxylithos 2[a]	4	182.6	8.3	−46.1	5.7	257.1	3.988	38.57	24.08
Oxylithos 1[a,b,c]	17	223.2	6.3	−37.9	4.9	52.7	16.697	38.58	24.09
Plaka	4	11.7	7.6	50.3	4.8	364.7	3.992	37.77	24.02
Skyros[b]	4	26.0	11.0	45.5	7.7	82.0	3.964	38.90	24.51
Megara[d]	4	18.6	16.5	45.3	11.5	65.3	3.954	38.05	23.16
Tinos dykes[e]	10	28.1	15.8	36.7	12.6	15.6	9.425	37.59	25.21
Central Greece	**9**	**24.4**	**7.9**	**50.4**	**5.0**	**106.7**	8.925	**38.50**	**23.50**

Notes: D: Fisher mean declination; Δ*D*: 95% confidence interval of *D*; *I*: Fisher mean inclination; Δ*I*: 95% confidence interval of *I*; *k*: Fisher precision parameter; α_{95}: apical angle of the region of 95% confidence of Fisher mean; *R*: resultant of ChRM unit vectors. Lat: locality latitude; Lon: locality longitude.

[a] Locality is excluded from grand mean direction due to uncertainties in structural corrections.
[b] Includes data from Kissel et al. (1986b).
[c] Includes data from Morris (1995).
[d] Data from Mattei et al. (2004).
[e] Recalculated from site-mean data of Avigad et al. (1998).

Least-squares fits from sedimentary samples were derived from 3 or more (usually 5–9) temperature steps above 240 °C. In the few cases where (a) vector endpoints were directionally clustered between 240 and 350 °C but became erratic above 350 °C without revealing an origin-trending demagnetization path, (b) a low-temperature component had been fully removed, and (c) the remanence direction was corroborated by ChRM directions from other specimens collected from the same outcrop, we forced a linear fit through the 240–350 °C cluster and the origin. In volcanic and plutonic samples, we calculated ChRM directions from linear fits to 10 or more vector endpoints above 400 °C. With the exception of the results from the Kymi Formation (Bradley, 2012), we did not include great circle paths in our calculated mean directions due to an observed increased likelihood of incomplete removal of viscous overprints in these specimens.

To facilitate inclusion of previously published data, we calculated site- and locality-mean directions using the traditional approach of applying Fisher statistics to paleomagnetic ChRM directions (Table 1, Supplementary Table 1). We rejected directional outliers that are inconsistent with the dispersion expected from paleosecular variation using the variable cutoff method of Vandamme (1994) applied to the combined specimen-level directional dataset at each locality (30 out of 672 total ChRM directions). These outliers typically occur within stratigraphic intervals characterized by transitional magnetic polarity. Because the distribution of virtual geomagnetic poles (VGPs) is commonly more Fisherian than the distribution of paleomagnetic directions (Deenen et al., 2011), we additionally calculated Fisher mean directions from the VGP distribution of all high-quality specimen-level demagnetizations at each locality (Supplementary Table 2).

The resulting mean directions typically differ from those of Table 1 by less than 0.5°, while the estimated error intervals on the declination and inclinations (ΔD_x and ΔI_x) are typically smaller than ΔD and ΔI respectively (the 95% confidence intervals estimated by Fisher statistics on ChRM directions) by 2–3°. For all localities except the igneous units of the Oxylithos volcanics and the Plaka granodiorite at Lavrion, we find that the apical angle of the region of 95% confidence of the Fisher mean on VGP directions ($A95$) lies between $A95_{min}$ and $A95_{max}$, which are the minimum and maximum limits of $A95$, respectively, explicable by the effects of paleosecular variation alone (Deenen et al., 2011). We assessed the age of remanence using a basic fold test at 95% confidence level (hereafter termed MFT95) (McElhinny, 1964) and a basic reversal test at 95% confidence level (MRT95) (McElhinny, 1964). Where the number of data points was sufficient, we applied the parametric reversal test at 95% confidence (PRT95) (Tauxe et al., 2009) and the parametric progressive unfolding test at 95% confidence (PFT95) (Tauxe et al., 2009) to site-mean datasets. Locality mean directions were tested for commonality using the method of McFadden and Lowes (1981) (Supplementary Table 3).

We interpret all vertical-axis rotations with respect to geographic north. While the expected vertical-axis rotation for the region of Central Greece in either African or European reference frames is between 2° and 4° clockwise for rocks that were magnetized during Middle Miocene to Pliocene time, as calculated from the polar wander paths of Besse and Courtillot (2002) and Torsvik et al. (2008), the prevalence of intracontinental deformation over much of the Aegean region during this time and the modern pattern of spatially distributed, opposite-sense rotations precludes a confident correction for large-scale plate motion.

3. Sampling and paleomagnetic results

We next discuss the local geology, age constraints, specific sampling strategy, paleomagnetic results, and stability tests for each locality. The age constraints for the sampled basins and previously reported paleomagnetic results in the region are summarized in Fig. 4. Representative demagnetizations are plotted as vector-endpoint orthogonal projections (Fig. 5), and site- and locality-mean directions are plotted on equal-area stereonets (Fig. 6).

3.1. Late Miocene–Pliocene Markopoulo basin

The Upper Miocene sedimentary sequence of the Markopoulo–Kapandriti region (Fig. 3; Ka) consists of debris flow conglomerates derived from the Attic–Cycladic massif, which are overlain by poorly dated Miocene marls, Upper Miocene (Vallesian) limestones and travertines, Turolian conglomerates bearing the Pikermian fauna, and Pliocene travertines (Katsikatsos, 2000; Papanikolaou and Papanikolaou, 2007). The basal debris flows are probably correlative with similar deposits exposed in the Kymi–Aliveri basin in Central Evia, which have an inferred Middle Miocene age (<13.5 Ma) based on radiometric dating of pyroclastic ejecta interbedded with the underlying fluvial sequence (Bradley, 2012).

We sampled four sections within the Vallesian marls and travertinous limestones, with two sections yielding interpretable demagnetizations and two sections yielding only very weakly magnetized specimens. The first section is exposed within a large roadcut south of Markopoulo (MAR14-19), and yielded $N=6$ site mean directions. The second section consists of lacustrine limestones exposed along the coastline west of Aghios Apostoli (MAR21-29), which yielded $N=7$ site mean directions. The MAR21-29 site-mean directions pass the MRT95 reversal test in geographic coordinates, but fail this test after tilt correction. The in-situ Fisher mean magnetic inclination (55.3 ± 5.5°) is consistent with both the present day locality latitude and the latitude predicted by regional plate reconstructions; this value increases to an untenably steep 68.0° upon tilt correction. The limestones therefore appear to carry a post-tilting magnetization, probably acquired during late diagenesis. While the MAR14-19 sites yield a locality-mean direction that is consistent with the other directions reported in this study, we discard these sites from further consideration due to their large within-site dispersion, overlap with the present-day field direction, and lack of reversed directions. We calculated a locality mean direction for the Markopoulo basin from the in-situ MAR21-29 site means, also incorporating the tilt-corrected site mean previously reported from the Nea Palatia–Kalamos region (Morris, 1995). Inclusion of both tilt-corrected and in situ site-mean directions into the locality mean is warranted by the differing interpretations of the nature of the remanence at these sites, and the interpretation that post-tilting

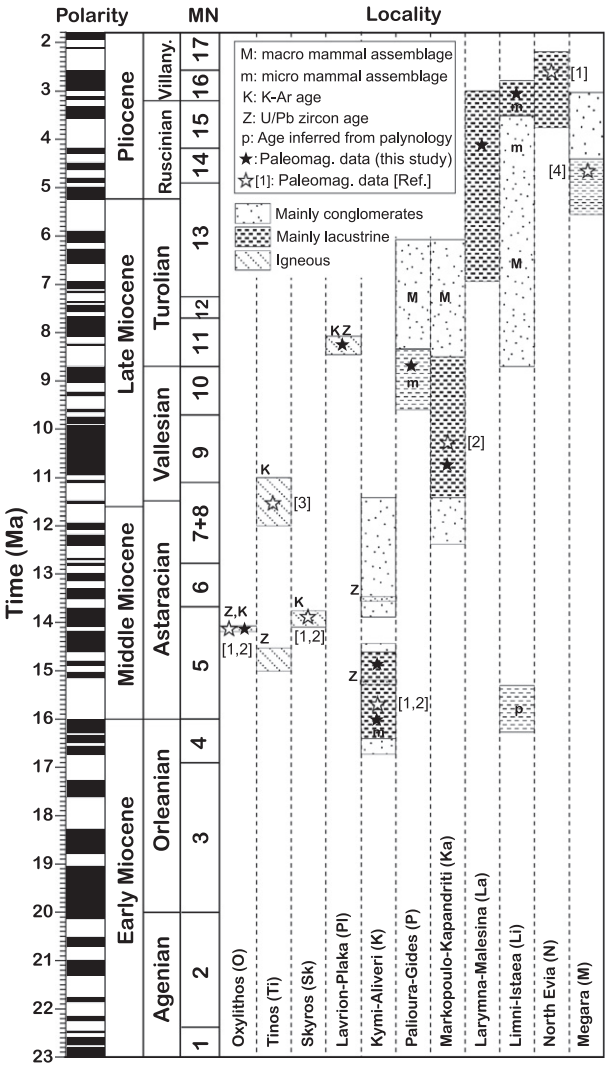

Fig. 4. Summary of Neogene sedimentary and igneous units of Central Greece discussed in this study. The magnetic polarity timescale is modified from Gee and Kent (2007), and European land mammal (MN) zones are modified from Böhme (2003). Age control is compiled from the paleontological and geochronological literature (Bolhar et al., 2010; Bradley, 2012; Fytikas et al., 1984; Guernet and Sauvage, 1969; Katsikatsos et al., 1981; Lemeille, 1977; Mettos, 1992). Previously-reported paleomagnetic site-mean data are from [1] Kissel et al. (1986b); [2] Morris (1995); [3] Avigad et al. (1998); [4] Mattei et al. (2004).

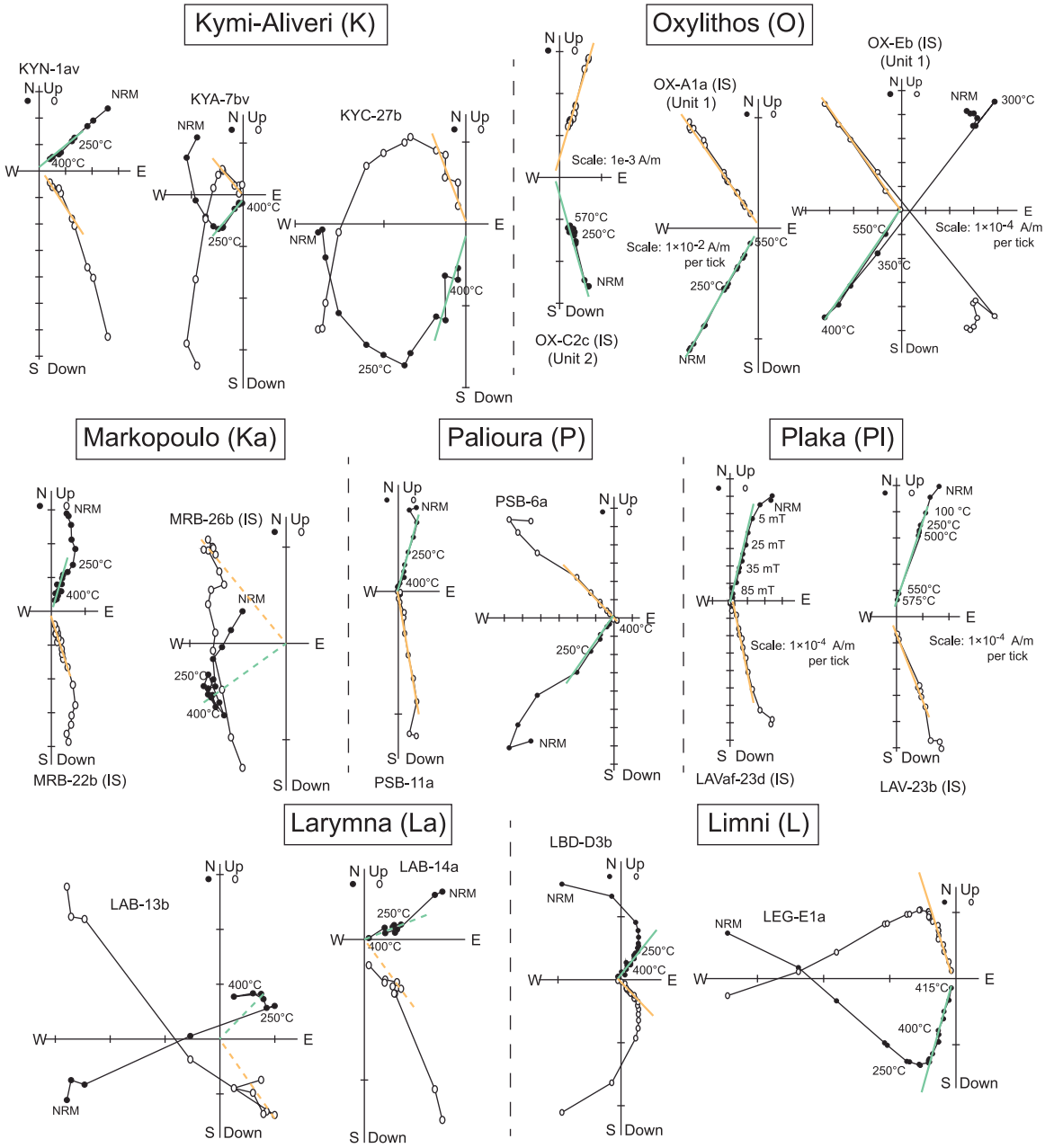

Fig. 5. Demagnetization behavior of representative specimens from each sampled locality, presented as orthogonal projections of vector endpoints after correction for local structural tilt (where appropriate). Green lines are least-squares fits projected onto the horizontal plane, and yellow lines are the same fits projected onto the vertical plane. Lines are dashed where fits are anchored to the origin due to lack of a high-quality origin-trending component. Scale: 1×10^{-6} A/m per tick unless otherwise noted. (For interpretation of the references to color in this figure legend, the reader is referred to the web version of this article.)

remagnetization of the MAR21-29 sites occurred prior to regional vertical-axis rotation.

3.2. Early–Middle Miocene Kymi Formation

The Kymi Formation is a thick (>700 m) sequence of lacustrine marls, siltstones, sandstones, and limestones that comprise the basal sequence of the Kymi–Aliveri basin (Fig. 3; K) and are well exposed along the northeastern coastline of Evia between Kymi and Stomio villages (Aronis, 1952; Deprat, 1904). Two composite sections that were previously sampled for magnetostratigraphy (Bradley, 2012) yielded high-quality demagnetizations (Figs. 5 and 6). Extrapolation of the inferred high sedimentation rate to the base of the lacustrine section yields an estimate for the onset of lacustrine deposition at $\sim 16.5 \pm 0.25$ Ma, and the youngest open-water lacustrine rocks are dated to $\sim 15.0 \pm 0.25$ Ma by correlation with the geomagnetic polarity timescale supported by radiometric dating of interbedded tephra deposits (Bradley, 2012).

While the full site-mean direction dataset fails the PRT95 reversal test in tilt-corrected coordinates, imposition of a strict selection criteria of $\alpha_{95} < 5.0^{\circ}$ ($N=24$; 13 normal, 10 reversed) yields a positive result (Fig. 7C) and a locality Fisher mean inclination of $56.8 \pm 4.8^{\circ}$. The results of the PFT95 fold test on the same restricted dataset are consistent with acquisition of magnetization between 93% and 126% unfolding (Fig. 7D); most of this folding is constrained to be of Middle Miocene age based on the pattern of angular unconformities mapped within the Kymi–Aliveri basin (Bradley, 2012). The restricted dataset yields an estimated net clockwise rotation of $23.6 \pm 8.7^{\circ}$ for the Kymi–Aliveri basin since ~ 15 Ma. This contrasts strongly with

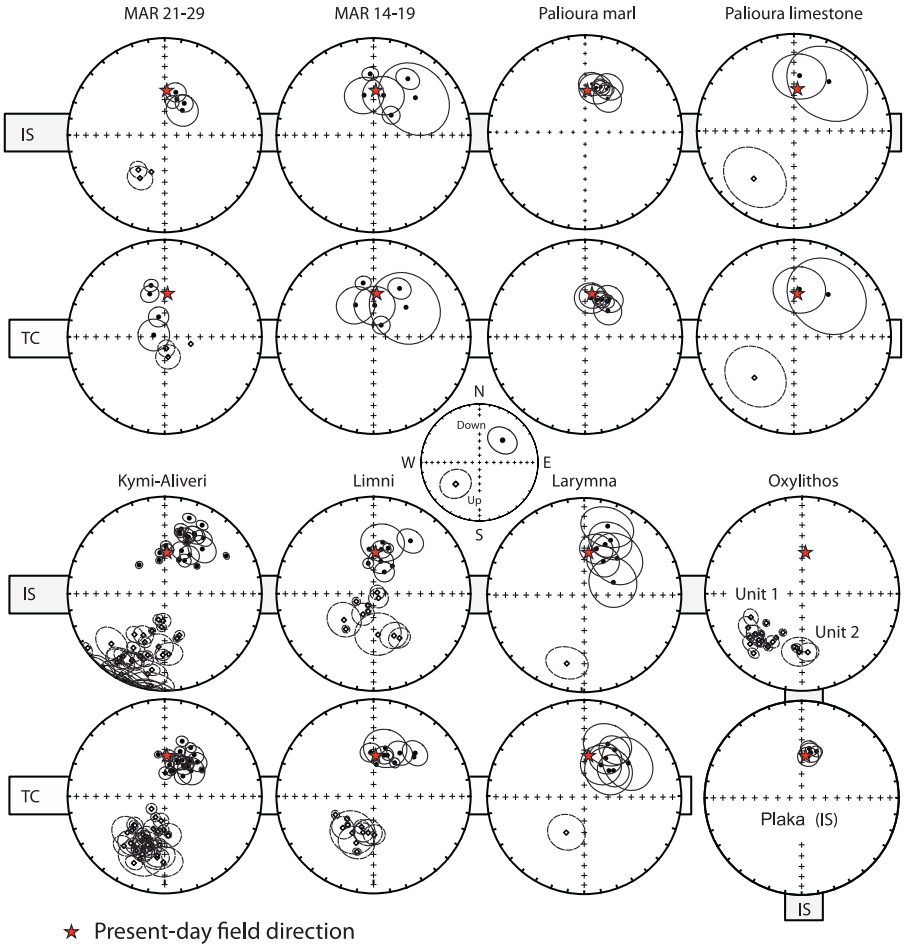

Fig. 6. Site mean directions from Neogene basins and volcanics in Central Greece measured in this study presented on equal-area stereonets with 95% angular confidence intervals. Where relevant, data are presented in both in-situ (IS) and tilt-corrected (TC) coordinates. Filled circles indicate downward-pointing vectors while open circles indicate upward-pointing vectors (legend at center). Stars indicate the present-day field direction.

previous estimates of up to $\sim 50^{\circ}$ of clockwise rotation derived from much smaller datasets from the Kymi Formation (Kissel et al., 1986a; Morris, 1995).

3.3. Middle Miocene Oxylithos volcanics

The Oxylithos volcanic massif (Fig. 3; O) consists of a shallowly intrusive, inflationary dome of white–green weathering magnesian dacites (Unit 1) that is overlain by potentially extrusive, red-weathering dacites and andesites (Unit 2) (Barbieri et al., 1998; Bradley, 2012; Deprat, 1904; Guernet, 1971; Pe-Piper and Piper, 1994). Two Unit 1 dacite samples yielded $^{238}U/^{206}Pb$ zircon crystallization ages of 14.097 ± 0.011 Ma and 14.105 ± 0.012 Ma (Bradley, 2012), interpreted as the time of intrusion of Unit 1 to shallow depth and synchronous eruption of Unit 2 respectively.

We sampled 7 sites at three Unit 1 sub-localities (OA, OB, OE) and four sites within two Unit 2 sub-localities (OC, OF). Samples from each site are located within ~ 3 m of each other, while each site is separated by >10–15 m in an effort to sample as much time difference as possible. All Unit 1 sites exhibit tightly-clustered, single-component reversed-polarity magnetizations (Fig. 6) that are consistent with previously reported measurements from the intrusive body (Kissel et al., 1986b; Morris, 1995). The Unit 2 sites also exhibit tightly-clustered reversed-polarity ChRM directions (Fig. 6), but preserve a mean direction that is statistically different from Unit 1 (Fig. 6). The single-component demagnetization paths and tight within-site clustering of ChRM directions (Fisher precision parameter $k > 200$ at most sites) indicate that cooling was rapid enough to record the instantaneous geomagnetic field direction. Several specimens exhibited multiple reversals in the direction of the removed NRM during thermal demagnetization that we interpret as self-reversed magnetizations arising from rock magnetic interaction effects (Nagata et al., 1957; Ozima et al., 1992).

Interpretation of the magnetization of the Oxylithos volcanics is complicated by an uncertain structural correction and potential undersampling of paleosecular variation. Previous paleomagnetic studies applied a tilt correction to the Oxylithos volcanics based on an inferred regional dip for the Kymi Formation under the assumption that the uppermost Kymi Formation sediments were deposited after emplacement of the volcanics and subsequently tilted (Kissel et al., 1986b; Morris, 1995). New geological mapping (Bradley, 2012) shows that the intrusive dacite body truncates an unconformity that cuts tilted lacustrine sediments of the Kymi Formation, indicating that the dacites were intruded into previously tilted beds. Additionally, geochronology and magnetostratigraphy of the Kymi Formation and Oxylithos volcanics shows that the volcanics postdate the end of lacustrine deposition by >1 Myr (Bradley, 2012). The 56 Oxylithos Unit 1 specimens measured in this study yield an $A95$ value of 2.2°, which is lower than the $A95_{min}$ value of 3.4° calculated from Deenen et al. (2011) for this number of specimens. This suggests that the Unit 1 rocks cooled too quickly to average paleosecular variation, indicating that the low inclination and large declination compared to the results from the Kymi Formation could simply reflect rapid acquisition of a non-representative field direction. Due to these uncertainties, we do not consider the magnetization of the Oxylithos volcanics as sufficiently reliable for tectonic interpretation.

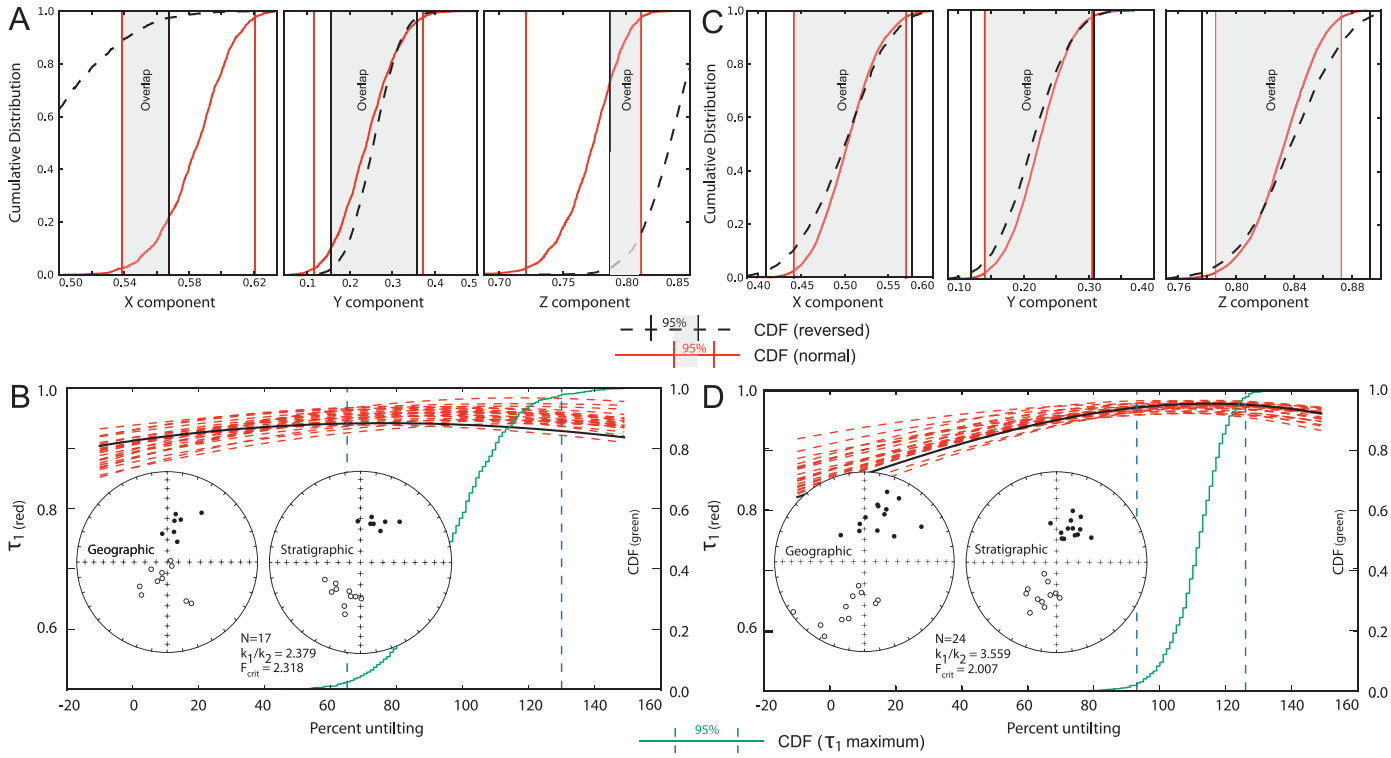

Fig. 7. Stability tests for the oldest (Kymi–Aliveri) and youngest (Limni–Istiaia) sedimentary sequences sampled in this study. Figures are modified from the output of the PmagPy software (Tauxe et al., 2009). (A,C) Result of PRT95 applied to the (A) Limni marls and (C) Kymi Formation (sites with $\alpha_{95} < 5^{\circ}$). Cumulative distribution and 95% confidence intervals for Cartesian magnetization components X,Y, Z are displayed for normal (red) and reversed (black) polarity directions. Overlap of 95% confidence intervals for normal and reversed directions on all three components (shaded regions) indicates a positive reversal test in both cases. (B,D) Result of PFT95 and MFT95 for the (B) Limni marls and (D) Kymi Formation (sites with $\alpha_{95} < 5^{\circ}$). Dashed red curves show the variation of the principal eigenvalue of the orientation matrix (τ_1) with percent unfolding for selected bootstrapped para-datasets. Green curve shows the cumulative distribution function for 1000 para-datasets. In both cases, the region of 95% confidence for the percent unfolding that maximizes τ_1 (vertical dashed lines) contains the 100% unfolding value. Lower-hemisphere equal area stereoplots show site-mean directions prior to (left) and after (right) correction for local bedding tilt. *N*: number of sites; k_1/k_2: ratio of Fisher precision parameters after and before tilt correction; F_{crit}: critical value of k_1/k_2 below which pre-tilting magnetization would be rejected at 95% confidence. (For interpretation of the references to color in this figure legend, the reader is referred to the web version of this article.)

3.4. Late Miocene Plaka granodiorite stock

The Plaka granodiorite stock in southeastern Attica (Fig. 3; Pl) was emplaced at shallow crustal levels within the Attic–Cycladic metamorphic massif as part of the Lavrion intrusive complex (Skarpelis et al., 2008). The emplacement age of this stock is constrained by an 8.27 ± 0.11 Ma K–Ar (biotite) cooling age (Altherr et al., 1982) and a U/Pb zircon crystallization age of 8.20 ± 0.20 Ma for a nearby granodiorite sill (Liati et al., 2009). We drilled 4 sites ($n=40$ specimens) in a fresh outcrop of non-hydrothermally altered granodiorite located within an incised gulley at the same locality as sample PLK7 in Skarpelis et al. (2008), thereby avoiding the effects of lightning remagnetization and surficial weathering.

Alternating field and thermal demagnetizations are equally efficient for the Plaka granodiorite specimens (Fig. 5). After removal of a weak present-day field overprint by 100 °C or 20 mT, all specimens yield a single origin-trending component, interpreted as a ChRM acquired during cooling during emplacement. With a single exception, ChRM directions have normal polarity and show tight within-site clustering. The resulting locality mean direction is not significantly different from the present-day field direction (Fig. 6). The *A*95 value of 3.7° is only marginally smaller than the $A95_{min}$ suggested by Deenen et al. (2011), indicating that paleosecular variation is underrepresented due to rapid cooling of the small intrusive stock. This direction cannot be corrected for post-magnetization tilting due to the lack of an appropriate paleohorizontal surface.

3.5. Pliocene Limni–Istiaia basin

The Limni–Istiaia basin (Fig. 3; Li) consists of <1 km of laterally-interfingering alluvial, fluvial, and lacustrine rocks exposed extensively over a forested area in North Evia (Guernet, 1971; Katsikatsos et al., 1981; Mettos, 1992). Lower Miocene lacustrine siltstones and clays exposed near Kerasia are unconformably overlain by fluvial conglomerates and sandstones bearing a MN11–MN12 (~9–7 Ma) mammal fauna (Theodorou et al., 2003). Near Limni, lacustrine marls depositionally overlie a thick sequence of coarse conglomerates bearing an Early Villanyian (MN16; ~3.4 Ma) rodent microfaunal association (Katsikatsos et al., 1981). This age is supported by the inferred age of a stratigraphically lower sequence that contains Early Ruscinian (MN14; ~4–5 Ma) fauna (Katsikatsos et al., 1981). The sampled beds are locally backtilted by 15–20° along an onland splay of the active Kandili normal fault system (Roberts and Jackson, 1991).

We collected samples from 23 sites ($n=110$ accepted specimens) from 7 separate sections (A–G) of the upper lacustrine marls exposed near Limni. Four sites yielded only non-interpretable demagnetizations, and three sites exhibited large scatter ($>15^{\circ}$) and were excluded from locality mean calculations. Most marl specimens exhibit linear demagnetization paths between 150 °C and ~450 °C, allowing for high quality least-squares fits (Fig. 5). Although the accepted site means fail PRT95, they pass this test when the LIM-A sites are not considered (Fig. 7A). We interpret the excess rotation of the LIM-A sites as resulting from localized block rotation. A pre-tilting age of

magnetization is supported by a positive site-mean MFT99 test and a positive PFT95 test that indicates acquisition of magnetization between 63% and 130% unfolding (Fig. 7B). The large number of sites and specimens and the positive stability tests make this result second only to that of the Kymi Formation (Section 3.2) in terms of reliability.

Two sites exhibiting within-site dispersal of $<10^{\circ}$ were previously reported from poorly-dated but probably Pliocene lacustrine limestones exposed near Lichada (Fig. 3; N) in northwestern Evia (Katsikatsos et al., 1981; Kissel et al., 1986b). The similarity of the in-situ site-mean directions to stable magnetizations measured from similar successions in this study, and the dissimilarity of the in-situ directions from the present local field and the expected dipole field directions suggest that these sites record post-tilting remagnetization. Due to this uncertainty in magnetization age, the low number of samples per site, and the lack of detailed geological context, we do not consider these previous results further.

3.6. Late Miocene Palioura–Gides basin

The Palioura–Gides basin (Fig. 3; P) consists of lacustrine marls, plastic clays, and thin lignite beds that are conformably overlain by fluvial–alluvial conglomerates, sandstones, and rare meter-thick palustrine limestones. Micromammal remains indicate a Late Vallesian (MN10; ~9–10 Ma) age for the uppermost marl beds (Katsikatsos et al., 1981), and mammal fauna collected by Deprat (1904) from the lowest conglomerate beds probably represents the Turolian (MN12; ~7–8 Ma) Pikermian fauna (Katsikatsos et al., 1981). This basin contains no major internal unconformities and is neither faulted nor folded, in contrast with the strongly-deformed $\sim 17-13$ Ma fill of the nearby Kymi–Aliveri basin.

We sampled 8 sites ($n=61$ accepted specimens) from ~40 m of gently-dipping clayey marls exposed in a fresh roadcut south of Aghios Athanasios, and we collected 3 sites ($n=15$ accepted specimens) from flat-lying sandstones and palustrine limestones of the upper sequence in the eastern basin. The sites drilled in marl yield internally consistent demagnetization paths that persist during heating to 400 °C, and occasionally to ~500 °C (Fig. 5). While these sites exhibit small within-site dispersion and appear reliable, no reversed-direction specimens were measured and the lack of small-scale post-depositional deformation precludes application of a fold test. However, both the in-situ and tilt-corrected mean directions yield similar mean declination and inclinations consistent with $\sim 20^{\circ}$ of clockwise vertical-axis rotation. The three sites drilled in palustrine limestones yield stable demagnetizations but large within-site scatter ($>25^{\circ}$; Fig. 6). Although a locality mean direction calculated from these three sites is consistent with the results from the marls, we prefer to exclude the results from the limestones from further discussion due to their low quality.

3.7. Late Miocene–Pliocene Larymna–Malesina basin

The Larymna–Malesina (or Martino) basin (Fig. 3; La) consists of lacustrine marls, siltstones, and limestones of Upper Miocene to Lower Pliocene age (Lemeille, 1977; Mettos, 1992). The basin sequence is gently back-tilted along the active Atalanti Fault and is cut by the north-dipping Malesina Fault (Ganas et al., 2006). The neighboring Lokris–Beoticos basin borders the modern Gulf of Evoikos and experienced fluvial–lacustrine sedimentation from latest Miocene to Pliocene time. The present fault-bounded steep topography does not predate Middle to Late Pleistocene time (Kranis, 2002), and the relationship of the oldest (Upper Miocene–Pliocene) sediments to the active, topographically pronounced fault systems remains uncertain.

We sampled four stratigraphic sections in the lacustrine deposits near Malesina. Most of the sampled beds consist of highly calcareous marls exhibiting very weak magnetizations, which resulted in a small number of accepted specimens per sampled bed and failure of all sites collected from two of the sections. Accepted specimens often require forcing of linear fits to the origin due to loss of magnetic stability above 350 °C (Fig. 5). While the within-bed magnetizations from the two sections that yielded reasonable demagnetization paths typically show large directional dispersion (Fig. 6), only four specimens were rejected by application of the Vandamme (1994) variable cutoff to the full specimen-level dataset. For this basin, we calculate site mean statistics using grouped specimens from continuously exposed outcrops with total stratigraphic separations of <20 m. The mean directions of sites with a large number of accepted specimens collected from a single bed are consistent with the mean directions of these grouped sites, validating this alternative approach. The single reversed site is insufficient for application of a reversal test. Structural correction of the highest quality sites yields an average magnetic inclination of $51.4 \pm 7.5^{\circ}$ (vs. 44.9° in-situ) that is at least not inconsistent with a pre-tilting magnetization for the latitude of Central Greece. While the site-mean directions from this locality are of relatively poor quality, their compatibility with the other locality mean directions reported in this study suggests that the inferred clockwise rotation of $35.4 \pm 12.0^{\circ}$ for the Larymna–Malesina basin is meaningful.

4. Rock magnetism

White, gray, and green-tinged lacustrine mudstone and marl comprise the majority of specimens analyzed in this study. Under thermal demagnetization, these specimens tend to fully unblock by ~400 °C, although many specimens exhibit erratic demagnetization paths and large increases in magnetization and magnetic susceptibility above 350–400 °C likely due to chemical alteration during heating. The presence of a magnetite fraction is indicated by persistence of magnetization to ~550 °C in some specimens. Alternating field demagnetization was ineffective for nearly all sedimentary specimens, which tended to acquire a laboratory-induced gyroremanent magnetization (GRM) of up to 5 times the NRM intensity above peak applied fields of ~150 mT (Supplemental Fig. 1).

We analyzed the coercivity distribution of 13 specimens using the cumulative log-Gaussian (CLG) approach to fit isothermal remanent magnetization (IRM) acquisition spectra (Kruiver et al., 2001). Most specimens were saturated below applied fields of 150 mT, although several showed continued acquisition at higher field intensities. The best fits were obtained using two or three components (Supplemental Table 3): a low-coercivity component with a mean acquisition field ($B_{1/2}$) between 26 and 63 mT (average 33 mT) and dispersion parameter (DP) between 0.31 and 0.54 (average 0.39), a medium-coercivity component with $B_{1/2}$ between 43 and 95 mT (average 62 mT) and DP between 0.19 and 0.30 (average 0.26), and in two samples a high-coercivity component with $B_{1/2}$ between 500 mT and 1000 mT and DP of 1.1–1.5 (Supplemental Fig. 2). After subtraction of a mass-specific paramagnetic component, hysteresis loops measured on an ADE 1660 VSM exhibit open forms with saturation remanent magnetization to saturation magnetization (M_{rs}/M_s) ratios of 0.3–0.4 and coercivity (B_c) values between 17 and 25 mT. We measured the coercivity of remanence (B_{cr}) on the 2G SRM using the backfield method on the same specimens; the resulting B_{cr}/B_c ratios range between 2 and 3. These data indicate that the mean grain size is pseudo single domain.

The combination of low-temperature unblocking and efficient acquisition of GRM suggests the presence of greigite (Fe_3S_4) as a

primary carrier of remanence. The low-dispersion IRM acquisition component centered at ~70 mT is similar to that seen in well-characterized greigite-bearing sediments (Vasiliev et al., 2007), while the weak high-coercivity component in some specimens probably indicates the presence of an unknown phase that probably reflects surface weathering. Greigite growth is favored in organic-rich sediments that experienced high deposition rates in a low-oxygen environment, a situation that is typical of many lacustrine settings. Heavy mineral separates of lacustrine rock samples from the Kymi–Aliveri basin contain abundant pyrite (FeS_2), indicating that iron sulfide growth was important during diagenesis. Diagenetic growth of greigite through decomposition of organic material can postdate burial by up to 0.3 Ma, resulting in a large time lag between initial depositional magnetization and subsequent grain-growth chemical remagnetization (Porreca et al., 2009; Roberts and Weaver, 2005). In this study, the greigite-borne magnetization is constrained by paleomagnetic tilt tests to predate regional deformation and the sediments are independently dated by mammal paleontology and radiochronology.

The Oxylithos dacites exhibit a complex magnetic mineralogy. Green and white weathering specimens collected from Unit 1 exhibit discrete ranges of enhanced unblocking during progressive heating between 300 and 350 °C, 400 and 450 °C, 510 and 525 °C, and 555 and 580 °C, indicating the presence of four distinct grain populations. Large (>100 μm) corroded magnetite grains are petrographically abundant within these rocks (Deprat, 1904). The red-weathering specimens collected from Unit 2 show minor unblocking between 400 and 450 °C (attributed to titanomaghemite) and show abundant euhedral magnetite grains in thin section (Deprat, 1904). These specimens maintain a strong remanence well above the maximum unblocking temperature of magnetite (585 °C), indicating that hematite is also a significant carrier of remanence in these rocks.

In summary, the sediments and volcanics measured in this study contain magnetic mineral populations that coincide with or slightly postdate deposition or emplacement and are capable of preserving stable magnetizations over geological timescales.

5. Discussion

5.1. Pliocene vertical-axis rotation of Central Greece

Each locality sampled in this study yielded a mean declination consistent with clockwise net rotation with respect to geographic north (Fig. 8). The Kymi Formation shares a true common true mean direction at 95% confidence (McFadden and Lowes, 1981) with the Limni–Istiaia, Palioura–Gides, and Markopoulo basins (Supplemental Table 4). Because these sequences range in depositional age from Early–Middle Miocene (Kymi–Aliveri) to Middle Pliocene (Limni–Istiaia) and appear to retain primary or early diagenetic magnetizations, we infer that clockwise rotation in Central Greece commenced in Early to Middle Pliocene time. This agrees with previously proposed scenarios that were based on the Pliocene age of paleomagnetic rotations in the Ionian Islands but were necessarily speculative due to incomplete data coverage in Central Greece (Kissel and Laj, 1988; Taymaz et al., 1991). Due primarily to the scatter in locality-mean inclinations, Fisher averages of the Middle Miocene and Pliocene locality-mean directions do not have small enough ΔD values to preclude some amount of vertical-axis rotation between ~15 and ~3 Ma. However, locality means calculated from specimen-level data have smaller ΔD values that admit very little vertical-axis

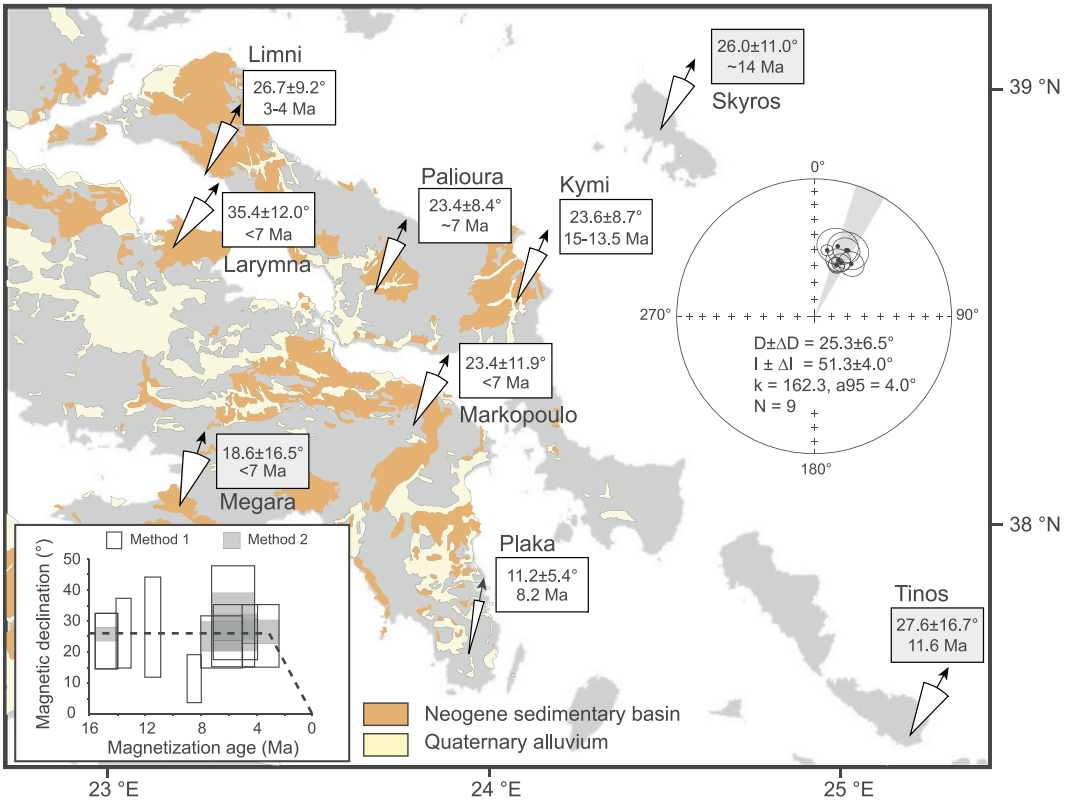

Fig. 8. Map showing the distribution of vertical-axis rotations inferred from paleomagnetism in Central Greece. Arrow points toward the normal-polarity Fisher mean declination. Wedge half-width is the 95% confidence interval for the Fisher mean declination (ΔD). Shaded boxes indicate a published locality-mean direction (references are given in the caption of Table 1). Inset: paleomagnetic declination vs. time for Central Greece. Unfilled boxes show 95% confidence intervals on locality-mean declinations calculated from site-mean directions (Method 1; Table 1); shaded boxes show 95% confidence intervals on locality-mean declinations calculated from the entire specimen-level dataset (Method 2; Supplementary Table 2).

rotation during this time (Fig. 8, inset). Furthermore, the scatter in data allows counter-clockwise rotations as easily as clockwise rotations.

The region of consistent paleomagnetic declinations extends beyond the study area. The Late Miocene (?) to Pleistocene Megara basin (Bentham et al., 1991) underwent a net clockwise rotation of $18.6 \pm 16.5^{\circ}$ in Plio-Pleistocene time, based on the paleomagnetism of four sites drilled in the poorly dated, basal lacustrine beds (Mattei et al., 2004). The ~14 Ma high-magnesium dacite body exposed on the nearby island of Skyros records a vertical-axis rotation of $26.0 \pm 11.0^{\circ}$ (Kissel et al., 1986b), and the island of Limnos exhibits a post-Early Miocene clockwise rotation of $34.0 \pm 22.8^{\circ}$ (Westphal and Kondopoulou, 1993). On Tinos, sites were previously drilled in a 14.73 ± 0.22 Ma monzogranite pluton (recently re-dated by Bolhar et al. (2010)) and a swarm of NW–SE trending, 11.55 ± 0.43 Ma post-detachment dacitic dykes (Avigad et al., 1998). The monzogranite yielded a poorly-constrained clockwise rotation of $26 \pm 37.6^{\circ}$, while the dykes record a better-constrained clockwise rotation of $28.1 \pm 15.8^{\circ}$ (Avigad et al., 1998). A locality-mean direction measured from a strained Middle Miocene pluton at Mykonos (Morris and Anderson, 1996) is also consistent with significant clockwise rotation; however, we consider this direction to be unreliable as the mean inclination is much too low. The apparent counter-clockwise rotation of Plio-Pleistocene sequences in the Gulf of Corinth (Mattei et al., 2004) suggests that this major fault zone could be the southwestern boundary of the Central Greece Block; however, a number of sites showing Plio-Pleistocene clockwise rotation have also been reported from the southern Peloponnesos (van Hinsbergen et al., 2005a, 2005b).

We calculate a grand mean direction for Central Greece (Table 1; bold) that incorporates our new results with the published locality mean directions from Skyros, Tinos (dykes only) (Avigad et al., 1998), the Plaka granodiorite, and the Megara basin (Mattei et al., 2004). We elect not to incorporate the Tinos monzogranite site-mean data due to their inadequate precision and small number of sites (Avigad et al., 1998). This grand-mean direction suggests that $25.3 \pm 6.5^{\circ}$ of post-Middle Pliocene clockwise rotation (relative to geographic north) occurred over a region at least 250 km long by 150 km wide, with an estimated mean rotation rate of ~8–10°/Myr. It remains uncertain whether this rotation reflects displacement of a single, internally-coherent crustal block that was subsequently fragmented by the active fault systems that presently define the Gulfs of Evoikos, or whether rotation was accommodated by a set of fault-bounded blocks (e.g. McKenzie and Jackson, 1983).

Geodetically constrained block models of the Aegean region indicate that Central Greece is part of a rigid block that extends as far west as the Adriatic–Aegean plate interface in Western Greece and Epirus (Nyst and Thatcher, 2004; Reilinger et al., 2010, 2006) (Fig. 2). Estimates of rotation rates obtained from the geodetic velocity field indicate clockwise rigid-body rotation rates of ~2–4°/Myr over most of Central Greece (Floyd et al., 2010; McClusky et al., 2000; Nyst and Thatcher, 2004; Reilinger et al., 2006; Rontogianni, 2010). The long-term (4 Myr) vertical-axis rotation rate therefore appears to exceed the geodetic rotation rate in Central Greece by a factor of two to four. The eastern boundary of the Central Greece block may coincide with the proposed (but submerged) Mirthes–Ikaria strike-slip fault (Philippon et al., 2011).

5.2. Vertical-axis rotation and regional crustal deformation

The North Aegean Sea region underwent N–S directed extension starting in late-Middle to Late Miocene time, as indicated by the development of marine and terrestrial basins bounded primarily by syn-sedimentary normal faults (Mascle and Martin, 1990; Snel et al., 2006). The record of Neotethyan marine incursion into the Paratethyan realm through the Marmara Sea region indicates that the modern trace of the North Anatolian Fault in the Aegean Sea was at low elevation since ~11 Ma, implying a history of crustal thinning that significantly predated the main period of offset on the North Anatolian Fault (Çağatay et al., 2006). This time period also saw N–S directed extension and subsidence in the Cretan Trough, final unroofing of the Attic–Cycladic Complex recorded by closure of zircon and apatite fission track chronometers (Philippon et al., 2011 and references therein), and eventual submergence of the previously subaerial nonvolcanic outer arc in southern Peloponnesos, Kythera, and Crete (Zachariasse et al., 2011). While the evidence for regional extension is clear, there are no paleomagnetic data that require vertical-axis rotation during this time, confirming that the western Hellenic Trench had not yet evolved into a differentially retreating boundary (McKenzie, 1978; Le Pichon et al., 1995).

Uplift of the nonvolcanic outer arc above sea level initiated in Early Pliocene time, coincident with the main phase of shortening within the Mediterranean Ridge accretionary prism (Le Pichon et al., 2002). In Western Greece, imbrication of the Paxos Zone and onset of rapid clockwise rotation initiated in Early Pliocene time (Duermeijer et al., 1999; Kissel and Laj, 1988; Mercier et al., 1989). Uplift above sea level of Crete, Karpathos, and Rhodos associated with sinistral strike-slip faulting also occurred between 5 and 3 Ma (van Hinsbergen et al., 2007; Zachariasse et al., 2008). These events appear to record an acceleration of trench retreat between the Kephalonia Fault and Rhodos, probably due to the combined effects of downward pull of the negatively-buoyant, subducted Ionian Sea lithosphere (Royden and Papanikolaou, 2011) and development of the main offset-bearing structures of the North Anatolian Fault system (Şengör et al., 2005).

To place the observed vertical-axis rotations into the framework of the larger-scale evolution of the Aegean geometric arc, we present a schematic palinspastic reconstruction for the Aegean region to Early Pliocene time (4 Ma). We generated this map by back-projecting the modern coastlines along the geodetic velocity field, followed by local adjustment to account for the pattern of regional vertical-axis rotations as constrained by paleomagnetism (Fig. 9). While the decadal velocity field is almost certainly not representative of the pattern of crustal deformation over this time period, there does appear to be a basic consistency between the velocity field and the tectonic evolution of the Aegean Sea region over the last several million years (Reilinger et al., 2010). This largely qualitative reconstruction is consistent with geological estimates of ~80 km of right-lateral offset across the North Anatolian Shear Zone since Pliocene time (Şengör et al., 2005), and with an estimated southwestward retreat of the Hellenic slab hinge of ~60 km south of the Kephalonia Fault (Pearce et al., 2012). Our proposed map at ~4 Ma is similar in plan form to the reconstruction of Le Pichon and Angelier (1979) at ~13 Ma, with the primary difference being the large post-Early Pliocene deformation required by the paleomagnetic rotations from Central Greece presented in this study.

This reconstruction brings the south-facing ocean–continent transition zone of Mesozoic age marking the southern boundary of the Adriatic platform into alignment with the Hellenic bathymetric trench during Early Pliocene time (Fig. 9). South of Kephalonia, the eastern trench escarpment coincides with a set of seismogenic high-angle thrust faults that splay off of a deep-seated, shallowly-dipping decollement representing the true plate interface (Shaw and Jackson, 2010). The southern Hellenic bathymetric trench may therefore represent the southern Adriatic continental margin that was reactivated as a system of high-angle thrust faults during Pliocene accelerated Aegea–Nubia convergence.

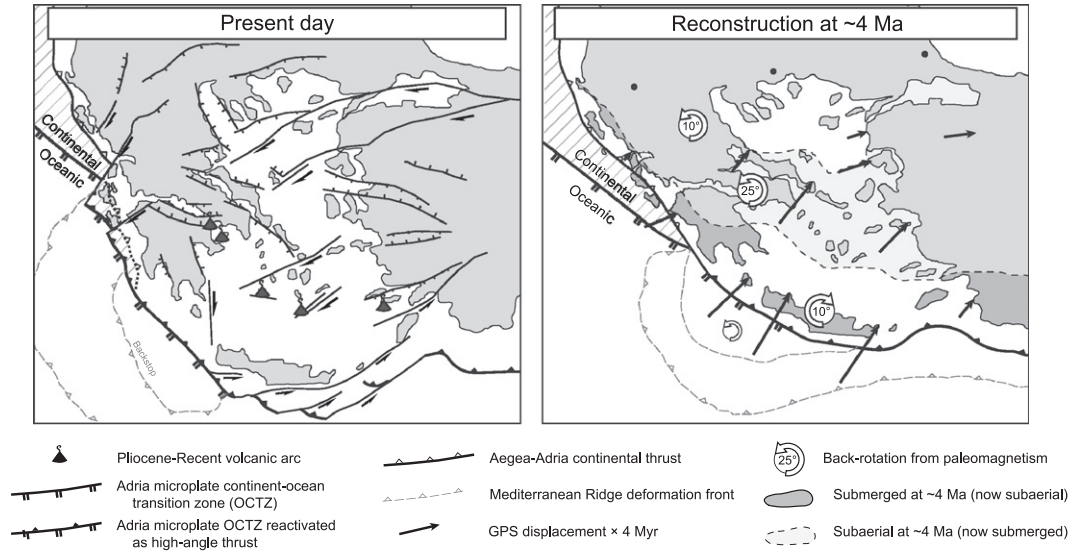

Fig. 9. Schematic paleogeographic evolution of the Aegean Sea region prior to initiation of the Central Hellenic Shear Zone, generated by back-projection of the present-day coastline (left) to 4 Ma (right) along the geodetic velocity field of Floyd et al. (2010) and local adjustments to reflect the observed pattern of post-Miocene paleomagnetic rotations.

5.3. Development of the Hellenic arc

The young rotation of the Central Greece Block provides a basic constraint on the earlier history of rotation in the External Hellenides of Western Greece, under the assumption that these regions were rigidly attached across the topographic Hellenides since Middle Miocene time. The Ionian Zone was folded and imbricated during Middle Miocene thrusting (Karakitsios and Rigakis, 2007; Le Pichon and Kreemer, 2010; Le Pichon et al., 2002; Meulenkamp, 1982), and was subsequently rotated clockwise by an average of 50° (Horner and Freeman, 1983; Kissel and Laj, 1988; van Hinsbergen et al., 2005a, 2006). While Middle Miocene (~17 Ma) sediments of the Klimatia–Paramythia basin and the northern Mesohellenic Trough are rotated by >50° in a clockwise sense (van Hinsbergen et al., 2005a), the ~16–15 Ma lacustrine deposits of the Kymi–Aliveri basin and the Middle Miocene (~14–13 Ma) igneous rocks of Skyros and Tinos only underwent ~25° of clockwise rotation after Early Pliocene time. Initial clockwise rotation of the External Hellenides and the Pelagonian Zone therefore occurred between ~17 and ~15 Ma, corresponding with the main period of thrusting around the Langhian–Burdigalian boundary (Karakitsios and Rigakis, 2007; Meulenkamp, 1982).

6. Conclusions

Vertical-axis rotation associated with a lateral gradient in the rate of trench retreat has commonly been envisioned as a progressive and generally continuous process occurring simultaneously with upper plate extension and southward-progressing arc magmatism above the dehydrating Hellenic slab (Jolivet and Brun, 2010; Ring et al., 2010; Royden and Papanikolaou, 2011). The paleomagnetic data presented here instead suggest a paroxysmal pattern of Aegean tectonics during Late Cenozoic time, with intervals of strong crustal deformation and rapid vertical-axis rotation in Middle Miocene and post-Early Pliocene time being separated by a period of apparent quiescence. The post-Early Pliocene onset of clockwise rotation in Central Greece indicates that connection of the North Anatolian Fault System to the Kephalonia–Achaia Fault Zone across the previously extended Aegean Sea region was directly associated with the initiation of rapid trench retreat along the southern Hellenic subduction zone.

Acknowledgments

This study was supported by the NSF Continental Dynamics Grant EAR-0409373 to L. Royden. A. Piasecki, J.S. Berdahl, L. Carporzen, and K. Soukis provided invaluable assistance in the field and the laboratory. B.P.W. also thanks the NSF Geophysics Program. We also thank L. Royden, B.C. Burchfiel, and D. Papanikolaou for many interesting discussions about Aegean tectonics.

Appendix A. Supporting information

Supplementary data associated with this article can be found in the online version at http://dx.doi.org/10.1016/j.epsl.2012.11.043.

References

Altherr, R., Kreuzer, H., Wendt, I., Lenz, H., Wagner, G., Keller, J., Harre, W., Hohndorf, A., 1982. A late Oligocene/early Miocene high temperature belt in the Attic–Cycladic crystalline complex (SE Pelagonian, Greece). Geol. Jahrb. 23, 97–164.

Amante, C., Eakins, B.W., Center, N.G.D., 2009. ETOPO1 1 arc-minute Global Relief Model: Procedures, Data Sources and Analysis. US Department of Commerce, National Oceanic and Atmospheric Administration, National Environmental Satellite, Data, and Information Service, National Geophysical Data Center, Marine Geology and Geophysics Division.

Angelier, J., Lyberis, N., Lepichon, X., Barrier, E., Huchon, P., 1982. The tectonic development of the Hellenic Arc and the Sea of Crete—a synthesis. Tectonophysics 86, 159–196.

Aronis, G.A., 1952. Aliveri—geological and mining survey of the lignite basin. Institute for Geology and Subsurface Research, Athens.

Avigad, D., Baer, G., Heimann, A., 1998. Block rotations and continental extension in the central Aegean Sea: palaeomagnetic and structural evidence from Tinos and Mykonos (Cyclades, Greece). Earth. Planet. Sci. Lett. 157, 23–40.

Barbieri, M., Castorina, F., Masi, U., Tucci, P., Azzaro, E., Kyriakopoulos, K., Magganas, A., Baltatzis, E., Collaceto, A., 1998. Elemental and Sr–Nd isotopic evidence for the origin and geodynamic significance of volcanic rocks from Oxylithos (Central Euboea, Greece). Bull. Geol. Soc. Greece 32, 251–258.

Bentham, P., Collier, R.E.L., Gawthorpe, R.L., Leeder, M.R., Prossor, S., Stark, C., 1991. Tectonosedimentary development of an extensional basin—the Neogene Megara Basin, Greece. J. Geol. Soc. London 148, 923–934.

Besse, J., Courtillot, V., 2002. Apparent and true polar wander and the geometry of the geomagnetic field over the last 200 Myr. J. Geophys. Res. 107, 1–31.

Böhme, M., 2003. The Miocene climatic optimum: evidence from ectothermic vertebrates of Central Europe. Palaeogeogr. Palaeocl. 195, 389–401.

Bolhar, R., Ring, U., Allen, C.M., 2010. An integrated zircon geochronological and geochemical investigation into the Miocene plutonic evolution of the Cyclades,

Aegean Sea, Greece: Part 1: Geochronology. Contrib. Mineral. Petrol. 160, 719–742.
Bradley, K., 2012. The Roof of the Cyclades: a Structural, Stratigraphic, and Paleomagnetic Investigation of Neogene Extension in Central Greece. Ph.D. Thesis. MIT, 302 pp.
Broadley, L., Platzman, E., Platt, J., Papanikolaou, M., Matthews, S., 2006. Paleomagnetism and the tectonic evolution of the Ionian zone, northwestern Greece. In: Dilek, Y., Pavlides, S. (Eds.), Geol. S. Am. S., 137–155.
Brun, J.P., Sokoutis, D., 2007. Kinematics of the southern Rhodope core complex (North Greece). Int. J. Earth Sci. 96, 1079–1099.
Çağatay, M.N., Görür, N., Flecker, R., Sakınç, M., Tünoğlu, C., Ellam, R., Krijgsman, W., Vincent, S., Dikbaş, A., 2006. Paratethyan–Mediterranean connectivity in the Sea of Marmara region (NW Turkey) during the Messinian. Sediment. Geol. 188, 171–187.
Cifelli, F., Mattei, M., Della Seta, M., 2008. Calabrian Arc oroclinal bending: the role of subduction. Tectonics 27, 15 pp.
Cogné, J., 2003. PaleoMac: a Macintosh™ application for treating paleomagnetic data and making plate reconstructions. Geochem. Geophys. Geosyst. 4, 1007.
Deenen, M.H.L., Langereis, C.G., van Hinsbergen, D.J.J., Biggin, A.J., 2011. Geomagnetic secular variation and the statistics of palaeomagnetic directions. Geophys. J. Int. 186, 509–520.
Deprat, J., 1904. Étude géologique et pétrographique de l'île d'Eubée, Thése, Muséum d'Histoire Naturelle, Paris, 230 pp.
Dewey, J.F., Şengör, A.M.C., 1979. Aegean and surrounding regions—complex multi-plate and continuum tectonics in a convergent zone. Geol. Soc. Am. Bull. 90, 84–92.
Duermeijer, C.E., Krijgsman, W., Langereis, C.G., Meulenkamp, J.E., Triantaphyllou, M.V., Zachariasse, W.J., 1999. A Late Pleistocene clockwise rotation phase of Zakynthos (Greece) and implications for the evolution of the western Aegean arc. Earth Planet. Sci. Lett. 173, 315–331.
Dupont-Nivet, G., Vasiliev, I., Langereis, C.G., Krijgsman, W., Panaiotu, C., 2005. Neogene tectonic evolution of the southern and eastern Carpathians constrained by paleomagnetism. Earth Planet. Sci. Lett. 236, 374–387.
Faccenna, C., Piromallo, C., Crespo-Blanc, A., Jolivet, L., Rossetti, F., 2004. Lateral slab deformation and the origin of the western Mediterranean arcs. Tectonics 23, 21 pp.
Floyd, M.A., Billiris, H., Paradissis, D., Veis, G., Avallone, A., Briole, P., McClusky, S., Nocquet, J.M., Palamartchouk, K., Parsons, B., England, P.C., 2010. A new velocity field for Greece: implications for the kinematics and dynamics of the Aegean. J. Geophys. Res.—Solid Earth 115, 25 pp.
Fytikas, M., Innocenti, F., Manetti, P., Peccerillo, A., Mazzuoli, R., Villari, L., 1984. Tertiary to Quaternary evolution of volcanism in the Aegean region. Geol. Soc. Spec. Publ. 17, 687.
Ganas, A., Sokos, E., Agalos, A., Leontakianakos, G., Pavlides, S., 2006. Coulomb stress triggering of earthquakes along the Atalanti Fault, central Greece: two April 1894 M6+ events and stress change patterns. Tectonophysics 420, 357–369.
Gee, J., Kent, D., 2007. Source of oceanic magnetic anomalies and the geomagnetic polarity timescale, in: Kono, M. (Ed.), Treatise on Geoyphysics 5, Elsevier, Amsterdam, pp. 455–507.
Goldsworthy, M., Jackson, J., Haines, J., 2002. The continuity of active fault systems in Greece. Geophys. J. Int. 148, 596–618.
Guernet, C., 1971. Études géologiques en Eubée et dans les régions voisines (Grèce), Mém. de la Faculté des Sciences de Paris, 395 pp.
Guernet, C., Sauvage, J., 1969. Sur la microflore des lignites et calcaires marneux des bassins Néogènes de Kymi et de Gides (Eubée, Grèce). C. R. Acad. Sci., 1611–1613.
Horner, F., Freeman, R., 1983. Paleomagnetic evidence from pelagic limestones for clockwise rotation of the Ionian Zone, Western Greece. Tectonophysics 98, 11–27.
Jolivet, L., Brun, J.P., 2010. Cenozoic geodynamic evolution of the Aegean. Int. J. Earth Sci. 99, 109–138.
Jones, C.H., 2002. User-driven integrated software lives. Comput. Geosci 28, 1145–1151.
Karakitsios, V., Rigakis, N., 2007. Evolution and petroleum potential of Western Greece. J. Petrol. Geol. 30, 197–218.
Katsikatsos, G., 2000. Geological map of Greece—Eretria Sheet. I.G.M.E., Athens, Greece.
Katsikatsos, G., De Bruijn, H., Van der Meulen, A., 1981. The Neogene of the island of Euboea (Evia), a review. Geol. Mijnbouw 60, 509–516.
Kirschvink, J., 1980. The least squares line and plane and the analysis of palaeomagnetic data. Geophys. J. R. Astron. Soc. 62, 699–718.
Kirschvink, J.L., Kopp, R.E., Raub, T.D., Baumgartner, C.T., Holt, J.W., 2008. Rapid, precise, and high-sensitivity acquisition of paleomagnetic and rock-magnetic data: development of a low-noise automatic sample changing system for superconducting rock magnetometers. Geochem. Geophys. Geosyst. 9, Q05Y01.
Kissel, C., 2003. Paleomagnetic reconstruction of the Cenozoic evolution of the Eastern Mediterranean. Tectonophysics 362, 199–217.
Kissel, C., Kondopoulou, D., Laj, C., Papadopoulos, P., 1986a. New paleomagnetic data from Oligocene formations of Northern Aegea. Geophys. Res. Lett. 13, 1039–1042.
Kissel, C., Laj, C., 1988. The Tertiary geodynamical evolution of the Aegean Arc—a paleomagnetic reconstruction. Tectonophysics 146, 183–201.
Kissel, C., Laj, C., Mazaud, A., 1986b. First paleomagnetic results from Neocene Formations in Evia, Skyros and the Volos Region and the deformation of Central Aegea. Geophys. Res. Lett. 13, 1446–1449.
Kondopoulou, D., Caputo, R., 1997. Palaeomagnetic evidence for non-rotational deformation along the Nea Anchialos Fault System, Central Greece. Ann. Geophys. 40, 823–831.
Kranis, H., 2002. Kinematics of active faults in Lokris, central Greece—block rotation within a crustal-scale shear zone? Geol. Carpath. 53, 157–159.
Kruiver, P.P., Dekkers, M.J., Heslop, D., 2001. Quantification of magnetic coercivity components by the analysis of acquisition curves of isothermal remanent magnetisation. Earth Planet. Sci. Lett. 189, 269–276.
Laj, C., Jamet, M., Sorel, D., Valente, J., 1982. First paleomagnetic results from Mio-Pliocene series of the Hellenic sedimentary arc. Tectonophysics 86, 45–67.
Le Pichon, X., 2003. The North Anatolian fault in the Sea of Marmara. J. Geophys. Res.—Solid Earth 108, 20 pp.
Le Pichon, X., Angelier, J., 1979. The Hellenic arc and trench system—key to the neotectonic evolution of the Eastern Mediterranean area. Tectonophysics 60, 1–42.
Le Pichon, X., Chamotrooke, N., Lallemant, S., Noomen, R., Veis, G., 1995. Geodetic determination of the kinematics of Central Greece with respect to Europe—implications for Eastern Mediterranean tectonics. J. Geophys. Res.—Solid Earth 100, 12675–12690.
Le Pichon, X., Kreemer, C., 2010. The Miocene-to-Present kinematic evolution of the Eastern Mediterranean and Middle East and its implications for dynamics. Annu. Rev. Earth Planet. Sci. 38, 323–351.
Le Pichon, X., Lallemant, S.J., Chamotrooke, N., Lemeur, D., Pascal, G., 2002. The Mediterranean Ridge backstop and the Hellenic nappes. Mar. Geol. 186, 111–125.
Lemeille, F., 1977. Etudes néotectoniques en Grèce centrale nord-orientale (Eubée centrale, Attique, Béotie, Locride) et dans les Sporades du Nord (île de Skiros). Thése, Univ. Paris XI, Centre d' Orsay, 173 pp.
Liati, A., Skarpelis, N., Pe-Piper, G., 2009. Late Miocene magmatic activity in the Attic–Cycladic Belt of the Aegean (Lavrion, SE Attica, Greece): implications for the geodynamic evolution and timing of ore deposition. Geol. Mag. 146, 732–742.
Mascle, J., Martin, L., 1990. Shallow structure and recent evolution of the Aegean Sea—a synthesis based on continuous reflection profiles. Mar. Geol. 94, 271–299.
Mattei, M., d'Agostino, N., Zananiri, I., Kondopoulou, D., Pavlides, S., Spatharas, V., 2004. Tectonic evolution of fault-bounded continental blocks: comparison of paleomagnetic and GPS data in the Corinth and Megara basins (Greece). J. Geophys. Res.—Solid Earth 109, B02106.
Mauritsch, H.J., Scholger, R., Bushati, S.L., Xhomo, A., 1996. Palaeomagnetic investigations in Northern Albania and their significance for the geodynamic evolution of the Adriatic–Aegean realm. Geol. Soc. Spec. Publ. 105, 265–275.
McClusky, S., Balassanian, S., Barka, A., Demir, C., Ergintav, S., Georgiev, I., Gurkan, O., Hamburger, M., Hurst, K., Kahle, H., Kastens, K., Kekelidze, G., King, R., Kotzev, V., Lenk, O., Mahmoud, S., Mishin, A., Nadariya, M., Ouzounis, A., Paradissis, D., Peter, Y., Prilepin, M., Reilinger, R., Sanli, I., Seeger, H., Tealeb, A., Toksoz, M.N., Veis, G., 2000. Global Positioning System constraints on plate kinematics and dynamics in the eastern Mediterranean and Caucasus. J. Geophys. Res.—Solid Earth 105, 5695–5719.
McElhinny, M., 1964. Statistical significance of the fold test in palaeomagnetism. Geophys. J. R. Astron. Soc. 8, 338–340.
McFadden, P.L., Lowes, F.J., 1981. The discrimination of mean directions drawn from Fisher distributions. Geophys. J. R. Astron. Soc. 67, 19–33.
McKenzie, D., 1978. Active tectonics of the Alpine–Himalayan belt: the Aegean Sea and surrounding regions. Geophys. J. R. Astron. Soc. 55, 217–254.
Mckenzie, D., Jackson, J., 1983. The relationship between strain rates, crustal thickening, paleomagnetism, finite strain and fault movements within a deforming zone. Earth Planet. Sci. Lett. 65, 182–202.
Mercier, J., Sorel, D., Vergely, P., Simeakis, K., 1989. Extensional tectonic regimes in the Aegean basins during the Cenozoic. Basin Res. 2, 49–71.
Mettos, A., 1992. Geological and Palaeogeographical Study of the Terrestrial Neogene and Quartenary Formations of NE Attica and SE Beotea. Ph.D. Thesis. University of Athens, 259 pp.
Meulenkamp, J., 1982. On the pulsating evolution of the Mediterranean. Episodes 1, 13–16.
Morris, A., 1995. Rotational deformation during Palaeogene thrusting and basin closure in eastern central Greece: palaeomagnetic evidence from Mesozoic carbonates. Geophys. J. Int. 121, 827–847.
Morris, A., Anderson, M., 1996. First palaeomagnetic results from the Cycladic Massif, Greece, and their implications for Miocene extension directions and tectonic models in the Aegean. Earth Planet. Sci. Lett. 142, 397–408.
Nagata, T., Uyeda, S., Ozima, M., 1957. Magnetic interaction between ferromagnetic minerals contained in rocks. Adv. Phys. 6, 264–287.
Nyst, M., Thatcher, W., 2004. New constraints on the active tectonic deformation of the Aegean. J. Geophys. Res.—Solid Earth 109, 23 pp.
Ozima, M., Funaki, M., Hamada, N., Aramaki, S., Fujii, T., 1992. Self-reversal of thermoremanent magnetization in pyroclastics from the 1991 eruption of Mt. Pinatubo, Philippines. J. Geomagn. Geoelectr. 44, 979–984.
Papanikolaou, D., Alexandri, M., Nomikou, P., Ballas, D., 2002. Morphotectonic structure of the western part of the North Aegean Basin based on swath bathymetry. Mar. Geol. 190, 465–492.
Papanikolaou, D., Papanikolaou, I., 2007. Geological, geomorphological, and tectonic structure of NE Attica and seismic hazard implications for the northern edge of the Athens plain. Bull. Geol. Soc. Greece 40, 425–438.
Papanikolaou, D.J., Royden, L.H., 2007. Disruption of the Hellenic arc: Late Miocene extensional detachment faults and steep Pliocene-Quaternary normal faults—or what happened at Corinth? Tectonics, 26.

Pe-Piper, G., Piper, D.J.W., 1994. Miocene magnesian andesites and dacites, Evia, Greece—adakites associated with subducting slab detachment and extension. Lithos 31, 125–140.
Pearce, F.D., Rondenay, S., Sachpazi, M., Charalampakis, M., Royden, L.H., 2012. Seismic investigation of the transition from continental to oceanic subduction along the western Hellenic Subduction Zone. J. Geophys. Res. 117, B07306.
Philippon, M., Brun, J.P., Gueydan, F., 2011. Deciphering subduction from exhumation in the segmented Cycladic Blueschist Unit (Central Aegean, Greece). Tectonophysics 524–525 , 116–134.
Platt, J.P., 2007. From orogenic hinterlands to Mediterranean-style back-arc basins: a comparative analysis. J. Geol. Soc. London 164, 297–311.
Porreca, M., Mattei, M., Di Vincenzo, G., 2009. Post-deformational growth of late diagenetic greigite in lacustrine sediments from southern Italy. Geophys. Res. Lett. 36, 6 pp.
Reilinger, R., McClusky, S., Paradissis, D., Ergintav, S., Vernant, P., 2010. Geodetic constraints on the tectonic evolution of the Aegean region and strain accumulation along the Hellenic subduction zone. Tectonophysics 488, 22–30.
Reilinger, R., McClusky, S., Vernant, P., Lawrence, S., Ergintav, S., Cakmak, R., Ozener, H., Kadirov, F., Guliev, I., Stepanyan, R., Nadariya, M., Hahubia, G., Mahmoud, S., Sakr, K., ArRajehi, A., Paradissis, D., Al-Aydrus, A., Prilepin, M., Guseva, T., Evren, E., Dmitrotsa, A., Filikov, S.V., Gomez, F., Al-Ghazzi, R., Karam, G., 2006. GPS constraints on continental deformation in the Africa–Arabia–Eurasia continental collision zone and implications for the dynamics of plate interactions. J. Geophys. Res.—Solid Earth 111, 26 pp.
Ring, U., Glodny, J., Will, T., Thomson, S., 2010. The Hellenic subduction system: high-pressure metamorphism, exhumation, normal faulting, and large-scale extension. Annu. Rev. Earth Planet. Sci. 38, 45–76.
Roberts, A.P., Weaver, R., 2005. Multiple mechanisms of remagnetization involving sedimentary greigite (Fe3S4). Earth Planet. Sci. Lett. 231, 263–277.
Roberts, S., Jackson, J., 1991. Active normal faulting in central Greece: an overview. Geol. Soc. Spec. Publ. 56, 125–142.
Rontogianni, S., 2010. Comparison of geodetic and seismic strain rates in Greece by using a uniform processing approach to campaign GPS measurements over the interval 1994–2000. J. Geodyn. 50, 381–399.
Rosenbaum, G., Lister, G.S., 2004. Neogene and Quaternary rollback evolution of the Tyrrhenian Sea, the Apennines, and the Sicilian Maghrebides. Tectonics 23, 17 pp.
Royden, L.H., 1993. Evolution of retreating subduction boundaries formed during continental collision. Tectonics 12, 629–638.
Royden, L.H., Husson, L., 2009. Subduction with variations in slab buoyancy: models and application to the Banda and Apennine systems. In: Lallemand, S., Funiciello, F. (Eds.), Subduction Zone Geodynamics, Springer, Berlin, pp. 35–45.
Royden, L.H., Papanikolaou, D.J., 2011. Slab segmentation and late Cenozoic disruption of the Hellenic arc. Geochem. Geophys. Geosyst. 12, Q03010.
Şengör, A.M.C., Tüysüz, O., İmren, C., Sakınç, M., Eyidoğan, H., Görür, N., Le Pichon, X., Rangin, C., 2005. The North Anatolian Fault: a new look. Annu. Rev. Earth Planet. Sci. 33, 37–112.
Shaw, B., Jackson, J., 2010. Earthquake mechanisms and active tectonics of the Hellenic subduction zone. Geophys. J. Int. 181, 966–984.
Skarpelis, N., Tsikouras, B., Pe-Piper, G., 2008. The Miocene igneous rocks in the basal unit of Lavrion (SE Attica, Greece): petrology and geodynamic implications. Geol. Mag. 145, 1–15.
Snel, E., Marunteanu, M., Meulenkamp, J., 2006. Calcareous nannofossil biostratigraphy and magnetostratigraphy of the Upper Miocene and Lower Pliocene of the Northern Aegean (Orphanic Gulf–Strimon Basin areas), Greece. Palaeogeogr. Palaeocl. 238, 125–150.
Speranza, F., Kissel, C., Islami, I., Hyseni, A., Laj, C., 1992. First paleomagnetic evidence for rotation of the Ionian zone of Albania. Geophys. Res. Lett. 19, 697–700.
Tauxe, L., Butler, R., Banerjee, S., Van der Voo, R., 2009. Essentials of Paleomagnetism. University of California, Berkeley.
Taymaz, T., Jackson, J., Mckenzie, D., 1991. Active tectonics of the North and Central Aegean Sea. Geophys. J. Int. 106, 433–490.
Theodorou, G., Athanassiou, A., Roussiakis, S., Iliopoulos, G., 2003. Preliminary remarks on the Late Miocene herbivores of Kerassiá (Northern Euboea, Greece). Deinsea 10, 519–530.
Torsvik, T.H., Müller, R.D., Van der Voo, R., Steinberger, B., Gaina, C., 2008. Global plate motion frames: toward a unified model. Rev. Geophys. 46 (RG3004), 44.
Ustaszewski, K., Schmid, S.M., Fuegenschuh, B., Tischler, M., Kissling, E., Spakman, W., 2008. A map-view restoration of the Alpine–Carpathian–Dinaridic system for the Early Miocene. Swiss J. Geosci. 101, S273–S294.
van Hinsbergen, D., Langereis, C., Meulenkamp, J., 2005a. Revision of the timing, magnitude and distribution of Neogene rotations in the western Aegean region. Tectonophysics 396, 1–34.
van Hinsbergen, D.J.J., Dekkers, M.J., Bozkurt, E., Koopman, M., 2010. Exhumation with a twist: paleomagnetic constraints on the evolution of the Menderes metamorphic core complex, western Turkey. Tectonics 29, 33 pp.
van Hinsbergen, D.J.J., Dupont-Nivet, G., Nakov, R., Oud, K., Panaiotu, C., 2008. No significant post-Eocene rotation of the Moesian Platform and Rhodope (Bulgaria): implications for the kinematic evolution of the Carpathian and Aegean arcs. Earth Planet. Sci. Lett. 273, 345–358.
van Hinsbergen, D.J.J., Hafkenscheid, E., Spakman, W., Meulenkamp, J.E., Wortel, R., 2005b. Nappe stacking resulting from subduction of oceanic and continental lithosphere below Greece. Geology 33, 325.
van Hinsbergen, D.J.J., Krijgsman, W., Langereis, C.G., Cornee, J.J., Duermeijer, C.E., Van Vugt, N., 2007. Discrete Plio-Pleistocene phases of tilting and counter-clockwise rotation in the southeastern Aegean arc (Rhodos, Greece): early Pliocene formation of the south Aegean left-lateral strike-slip system. J. Geol. Soc. London 164, 1133–1144.
van Hinsbergen, D.J.J., van der Meer, D.G., Zachariasse, W.J., Meulenkamp, J.E., 2006. Deformation of western Greece during Neogene clockwise rotation and collision with Apulia. Int. J. Earth Sci. 95, 463–490.
Vandamme, D., 1994. A new method to determine paleosecular variation. Phys. Earth Planet. Inter. 85, 131–142.
Vasiliev, I., Dekkers, M.J., Krijgsman, W., Franke, C., Langereis, C.G., Mullender, T.A.T., 2007. Early diagenetic greigite as a recorder of the palaeomagnetic signal in Miocene-Pliocene sedimentary rocks of the Carpathian foredeep (Romania). Geophys. J. Int. 171, 613–629.
Vassilakis, E., Royden, L., Papanikolaou, D., 2011. Kinematic links between subduction along the Hellenic trench and extension in the Gulf of Corinth, Greece: a multidisciplinary analysis. Earth Planet. Sci. Lett. 303, 108–120.
Weil, A.B., Sussman, A.J., 2004. Classifying curved orogens based on timing relationships between structural development and vertical-axis rotations, in: Sussman, A., Weil, A. (Eds.), Paleomagnetic and Structural Analysis of Orogenic Curvature, Spec. Pap. Geol. Soc. Am. 383, pp.1–17.
Westphal, M., Kondopoulou, D., 1993. Paleomagnetism of Miocene volcanics from Lemnos island: implications for block rotations in the vicinity of the north Aegean Trough. Ann. Tecton. 7, 142–149.
Zachariasse, W.J., van Hinsbergen, D.J.J., Fortuin, A.R., 2008. Mass wasting and uplift on Crete and Karpathos during the early Pliocene related to initiation of south Aegean left-lateral, strike-slip tectonics. Geol. Soc. Am. Bull. 120, 976–993.
Zachariasse, W.J., van Hinsbergen, D.J.J., Fortuin, A.R., 2011. Formation and fragmentation of a late Miocene supradetachment basin in central Crete: implications for exhumation mechanisms of highpressure rocks in the Aegean forearc. Basin Res. 23, 678–701.

Supplementary Text for:
K. Bradley et al. (2012) Segmentation of the Hellenides recorded by Pliocene initiation of clockwise block rotation in Central Greece, *Earth Planet. Sci. Lett.*

S.1. References for paleomagnetic data included in Figure 2.

Atzemoglou et al. (1994), Avigad et al. (1998), Bobier (1968), Broadley et al. (2006), Duermeijer et al. (1998), Duermeijer et al. (1999), Duermeijer et al. (2000), Edel et al. (1991), Edel et al. (1992), Feinberg et al. (1994), Gürsoy et al. (2003), Haubold et al. (1997), Horner and Freeman (1983), Jordanova et al. (2001), Kaymakci et al. (2007), Kissel and Poisson (1987), Kissel et al. (1985), Kissel et al. (1986a), Kissel et al. (1986b), Kissel et al. (1987), Kondopoulou (1982), Kondopoulou (1994), Kondopoulou and Caputo (1997), Kondopoulou and Lauer (1984), Kondopoulou and Pavlides (1990), Kondopoulou and Westphal (1986), Kondopoulou et al. (2007), Laj et al. (1982), Lovlie et al. (1989), Marton et al. (1990), Marton et al. (2003), Mattei et al. (2004), Mauritsch et al. (1996), Morris (1995), Morris (2000), Morris and Anderson (1996), Morris and Robertson (1993), Muttoni et al. (1995), Muttoni et al. (1997), Piper et al. (2006), Pucher et al. (1974), Sen et al. (1986), Spais (1987), Speranza et al. (1992), Speranza et al. (1995), Surmont (1989), Tozzi et al. (1988), Turnell (1988), van Hinsbergen et al. (2005), van Hinsbergen et al. (2008), van Hinsbergen et al. (2010a), van Hinsbergen et al. (2010b), Westphal and Kondopoulou (1993), Westphal et al. (1991)

Supplementary Table 1. Site mean directions.

Locality	N_c	N_a	D_g(°)	I_g(°)	D_s(°)	I_s (°)	k	α_{95}(°)	Lat (°N)	Lon (°E)
Larymna (La)										
LAR1[a]	6	0	–	–	–	–	–	–	38.62	23.23
LAR2-6	23	10	66.3	63.2	**43.1**	**59.5**	6.85	19.9	38.62	23.23
LAR7-16	50	13	22.5	43.0	**32.8**	**41.7**	12.27	12.3	38.64	23.26
LAR17[a]	6	0	–	–	–	–	–	–	38.64	23.26
LAR18	7	7	29.3	57.1	**47.9**	**56.6**	21.50	13.3	38.64	23.26
LAR19-20	7	5	14.8	49.2	**29.1**	**52.3**	34.25	13.3	38.64	23.26
LAR21	5	5	41.8	47.8	**52.4**	**42.2**	13.42	21.7	38.60	23.21
LAR22-24[a]	17	0	–	–	–	–	–	–	38.60	23.21
LAR25-28	22	4	18.8	25.9	**24.0**	**40.0**	24.62	18.9	38.60	23.21
LAR-29[a]	5	0	–	–	–	–	–	–	38.60	23.21
LAR30	6	5	25.7	37.4	**27.7**	**59.3**	21.73	16.8	38.60	23.21
LAR31-33[b]	16	7	194.3	-28.1	**206.8**	**-56.3**	16.36	15.4	38.60	23.21
Markopoulo (Ka) (MAR14-19: roadcut, MAR21-29: coastal section)										
MAR-14[a]	4	4	346.7	55.2	330.6	59.1	34.23	15.9	38.28	23.82
MAR-15[a]	4	4	14.1	55.1	2.1	63.5	31.00	16.8	38.28	23.82
MAR-16[a]	3	3	48.2	41.7	47.7	52.7	17.99	30.0	38.28	23.82
MAR-17[a]	6	6	41.4	67.6	33.2	78.3	80.36	7.5	38.28	23.82
MAR-18[a]	5	5	356.9	36.9	349.1	42.9	150.9	6.3	38.28	23.82

MAR-19[a]	5	5	31.3	32.5	28.3	42.8	69.54	9.2	38.28	23.82
MAR-21[a]	4	2	199.9	-56.9	105.2	-67.3	21.74	56.5	38.30	23.89
MAR-22	6	6	**14.5**	**52.4**	343.0	72.5	63.86	8.5	38.30	23.89
MAR-23,24	10	4	**209.9**	**-47.6**	170.5	-72.9	81.62	10.2	38.30	23.89
MAR-25	5	4	**35.4**	**64.4**	279.5	80.7	48.73	13.3	38.30	23.89
MAR-26	6	6	**217.3**	**-53.1**	172.0	-80.2	91.54	7.0	38.30	23.89
MAR-27[a]	6	0	–	–	–	–	–	–	38.30	23.89
MAR-28	5	5	**31.5**	**58.4**	340.8	51.4	109.3	7.4	38.30	23.89
MAR-29	5	5	**18.6**	**57.8**	345.1	44.4	191.2	5.6	38.30	23.89
Nea Palatia[d]	–	5	358.9	62.4	**26.1**	**51.8**	331	4.2	38.3	23.8
Oxylithos (O) Unit 1										
A1	9	9	**213.2**	**-36.0**	–	–	1,788	1.2	38.60	24.1
A2	9	9	**220.5**	**-36.8**	–	–	607.7	2.1	38.60	24.1
A3	6	6	**210.6**	**-46.4**	–	–	2,602	1.3	38.60	24.1
B1	9	9	**223.1**	**-35.1**	–	–	75.72	6.0	38.59	24.11
B2	9	9	**230.2**	**-30.9**	–	–	239.9	3.3	38.59	24.11
B3	6	6	**226.0**	**-26.5**	–	–	118.6	6.2	38.59	24.11
E	8	8	**211.4**	**-41.5**	–	–	111.3	5.2	38.58	24.1
EU220[c]	–	7	**228.3**	**-37**	–	–	949	1.7	38.59	24.11
EU221[c]	–	7	**230.8**	**-50.6**	–	–	320	2.9	38.59	24.11
EU222[c]	–	6	**229.5**	**-36.2**	–	–	63	7.2	38.59	24.11
EU223[c]	–	9	**225.6**	**-41.3**	–	–	320	2.6	38.59	24.11
EU224[c]	–	10	**245.3**	**-41.5**	–	–	45	6.5	38.59	24.11
EU225[c]	–	10	**206.4**	**-53.3**	–	–	201	3.1	38.59	24.11
AN03[d]	–	8	**237.9**	**-34.7**	–	–	42	8.6	38.59	24.11
AN04[d]	–	11	**220.7**	**-32.4**	–	–	354	2.4	38.59	24.11
AN05[d]	–	5	**219.2**	**-22**	–	–	318	4.3	38.59	24.11
AN07[d]	–	9	**212.7**	**-35.3**	–	–	204	3.6	38.60	24.11
Oxylithos (O) Unit 2										
C1	9	9	**188.2**	**-43.9**	–	–	444.8	2.4	38.57	24.08
C2	7	7	**174.4**	**-39.3**	–	–	52.75	8.4	38.57	24.08
C3	9	9	**185.3**	**-43.1**	–	–	173.7	3.9	38.57	24.08
F	4	4	**182.9**	**-39.6**	–	–	48.26	13.4	38.58	24.08
Limni-Istiaia (Li)										
LIM-A1	6	6	207.0	-70.6	**224.3**	**-52.6**	52.57	9.3	38.77	23.31
LIM-A2	8	8	196.9	-74.6	**222.2**	**-57.5**	547.9	2.4	38.77	23.31
LIM-A3	10	8	246.0	-74.2	**244.3**	**-54.2**	254.3	3.5	38.77	23.31
LIM-A4[a]	6	–	–	–	–	–	–	–	38.77	23.31
LIM-A5	8	5	205.7	-79.3	**229.7**	**-60.8**	1,313	2.1	38.77	23.31
LIM-A6[a]	10	–	–	–	–	–	–	–	38.77	23.31

LIM-A7,8	8	5	12.7	62.0	**31.2**	**46.7**	55.45	10.4	38.77	23.31
LIM-A9	4	4	350.1	64.0	**18.6**	**53.2**	431.6	4.4	38.77	23.31
LIM-B1	6	6	149.6	-46.0	**178.8**	**-57.4**	60.00	8.7	38.78	23.31
LIM-B2[a]	7	5	173.7	-55.1	210.1	-54.2	17.97	18.6	38.78	23.31
LIM-B3[b]	8	6	154.0	-50.3	**188.4**	**-58.9**	36.00	11.3	38.78	23.31
LIM-C1	8	6	10.1	45.2	**13.7**	**47.4**	16.29	17.1	38.79	23.29
LIM-C2	7	6	10.0	51.7	**14.4**	**53.9**	76.53	7.7	38.79	23.29
LIM-D1[a]	8	2	354.2	51.9	5.0	63.1	23.69	53.8	38.78	23.28
LIM-D2	8	7	17.8	49.2	**32.3**	**56.4**	199.8	4.3	38.78	23.28
LIM-D3	8	6	34.9	33.9	**43.9**	**38.1**	42.30	10.4	38.78	23.28
LIM-E1	8	8	218.0	-51.8	**196.7**	**-40.3**	299.0	3.2	38.78	23.27
LIM-E2	8	8	228.5	-56.6	**200.4**	**-47.6**	15.75	14.4	38.78	23.27
LIM-E3	6	6	26.4	69.6	**356.2**	**52.6**	65.07	8.4	38.78	23.27
LIM-F1[a]	Samples disintegrated during transport								38.78	23.27
LIM-F2	7	6	130.5	-84.5	**196.1**	**-58.2**	66.81	8.3	38.79	23.26
LIM-F3	9	9	70.4	-86.7	**201.4**	**-62.3**	72.73	6.1	38.79	23.26
LIM-G1[a]	10	0	–	–	–	–	–	–	38.79	23.26
LIM-G2[a,b]	7	2	34.2	61.7	45.8	41.5	9.69	92.0	38.81	23.29
Palioura-Gides (P) (PS1-4 = upper conglomeratic unit, PS5-13 = lower marl unit)										
PS-1	6	0	–	–	–	–	–	–	38.52	23.8
PS-2[a]	8	4	35.3	37.7	39.0	43.2	8.9	32.6	38.52	23.8
PS-3[a]	6	4	5.8	42.2	6.6	49.1	20.6	20.8	38.52	23.8
PS-4[a]	12	5	220.1	-36.0	224.0	-41.1	9.9	25.5	38.52	23.8
PS-5	6	4	19.3	49.3	**23.6**	**55.4**	164.7	7.2	38.60	23.8
PS-6[a]	3	1	214.7	2.4	213.7	-32.4	–	–	38.60	23.8
PS-7	9	7	26.7	48.9	**32.0**	**54.5**	107.7	5.8	38.60	23.8
PS-8	12	11	18.9	48.9	**23.1**	**55.1**	71.5	5.4	38.60	23.8
PS-9	5	5	27.5	46.1	**32.3**	**51.7**	45.2	11.5	38.60	23.8
PS-10	9	5	33.5	55.7	**41.2**	**60.9**	44.7	11.6	38.60	23.8
PS-11	10	10	14.1	50.7	**17.6**	**57.2**	213.0	3.3	38.60	23.8
PS-12	7	4	7.8	48.4	**10.0**	**55.1**	78.7	10.4	38.60	23.8
PS-13	9	7	13.6	51.9	**8.5**	**56.7**	21.5	13.3	38.60	23.8
Plaka (Pl)										
LAV-1	10	10	**11.2**	**50.7**	–	–	33.05	8.5	37.77	24.02
LAV-2[b]	10	10	**17.7**	**48.4**	–	–	103.34	4.8	37.77	24.02
LAV-3	7	7	**8.9**	**54.7**	–	–	52.30	8.4	37.77	24.02
LAV-4	12	12	**8.8**	**47.3**	–	–	40.66	6.9	37.77	24.02

Notes: Paleomagnetic site-mean directions for localities discussed in the text. N_c: Number of collected specimens; N_a: Number of specimens accepted in Fisher mean direction; D_g, I_g: Fisher mean declination, inclination in geographic coordinates (bold indicates accepted mean direction);

D_s, I_s: Fisher mean declination, inclination after tilt correction (bold indicates accepted mean direction); k: Fisher precision parameter; α_{95}: apical angle of the region of 95% confidence of Fisher mean direction.
[a]Site is excluded from locality mean calculation (see section 3 in main text for discussion of exclusion criteria at each locality).
[b]Site contains both normal and reversed-polarity specimens.
[c]Site mean direction from Kissel et al. (1986b);
[d]Site mean direction from Morris (1995).

Supplementary Table 2.

Locality	Na/Nb	D[b]	ΔD_x[b]	I[b]	ΔI_x[b]	k	α_{95}[b]	K	$A95_{min}$[b]	$A95$[b]	$A95_{max}$[b]
Markopooulo[a]	32/32	26.8	6.2	55.8	3.5	55.1	3.5	33.4	4.3	4.5	10.2
Larymna	57/61	35.5	7.6	51.4	7.0	12.6	5.5	9.5	3.4	6.5	6.9
Kymi	300/310	25.2	2.1	52.8	1.9	26.6	1.6	21.8	1.7	1.8	2.2
Limni	119/127	26.3	3.9	54.3	3.3	24.4	2.7	17.1	2.5	3.2	4.2
Palioura	67/75	25.1	4.8	54.0	4.0	26.8	3.4	20.4	3.2	3.9	6.2
Oxylithos 2[a]	28/29	184.0	2.7	-41.7	3.3	105	2.7	123.7	4.5	2.5	11.2
Oxylithos 1[a]	56/56	219.9	2.3	-36.2	3.2	69.9	2.3	75.7	3.4	2.2	7.0
Plaka[a]	40/40	11.2	4.3	49.5	4.2	43.8	3.5	38.9	3.9	3.7	8.7

Notes: Locality mean directions calculated using Fisher statistics on specimen-level ChRM directions transformed to virtual geomagnetic pole (VGP) directions. N_a: Number of specimens after iterative exclusion of outliers; N_b: Number of specimens before iteration; ΔD_x: Interval of 95% confidence on the declination; ΔI_x: Interval of 95% confidence on the inclination; A95: Fisher angular error on VGP directions; $A95_{min}$: minimum value of A95 expected for a dataset of N directions that adequately sample paleosecular variation, calculated from $A95_{min} = 17 \times N^{-0.4}$ (Deenen et al., 2011); $A95_{max}$: maximum value of A95 expected for a dataset of N specimens with a dispersion reflecting only paleosecular variation.
[a]Locality is not corrected for structural tilt.
[b]Units are degrees (°).

Supplementary Table 3. Results of quantitative coercivity analysis

ID	S_1[a]	C_1[b]	D_1[c]	S_2[a]	C_2[b]	D_2[c]	S_3[a]	C_3[b]	D_3[c]	S-Ratio
K14b	466	1.60	0.41	1300	1.70	0.27	–	–	–	0.989
K15b	173	1.43	0.54	1460	1.64	0.30	–	–	–	0.990
K17b	4520	1.70	0.41	8850	1.79	0.23	–	–	–	0.979
K18b	11800	1.76	0.37	8280	1.90	0.20	–	–	–	0.967
K14a	3160	1.51	0.34	4580	1.94	0.22	1310	2.75	1.10	0.933
P11b	626	1.69	0.42	497	1.98	0.16	–	–	–	0.966
PA3b	–	–	–	2170	1.60	0.35	100	2.75	0.50	0.953
PA6b	287	1.48	0.31	378	1.86	0.23	198	2.97	1.49	0.931
PA5b	1650	1.80	0.36	1430	1.85	0.19	–	–	–	0.968
LBDb	182	1.10	0.49	1530	1.75	0.30	–	–	–	0.985
LEGe	500	1.25	0.40	1800	1.72	0.34	–	–	–	0.979
LMAa	226	1.30	0.50	1670	1.68	0.33	–	–	–	0.984

LBDc	980	1.55	0.31	1810	1.86	0.24	–	–	–	0.994

Notes: Distribution parameters of Gaussian components inferred from IRM acquisition spectra for Neogene lacustrine sediments from Central Greece.
[a]Relative contribution to the magnetization (Am^2/kg)
[b]Mean acquisitive field (mT)
[c]Dispersion parameter (unitless)

Supplementary Table 4. Test of true common mean direction (McFadden and Lowes, 1981)

	Larymna	Lavrion	Limni	Palioura	Mark.	Tinos[a]	Skyros[a]	Megara[a]	Oxy[a]
Kymi	Fail	Fail	Pass	Pass	Pass	Pass	Fail	Fail	Fail
Larymna		Fail	Pass	Fail	Pass	Fail	Pass	Fail	Fail
Lavrion			Fail	Fail	Fail	Fail	Fail	Pass	Fail
Limni				Pass	Pass	Fail	Pass	Fail	Fail
Palioura					Pass	Fail	Fail	Fail	Fail
Markopoulo						Fail	Fail	Fail	Fail
Tinos[a]							Pass	Pass	Fail
Skyros[a]								Pass	Fail
Megara[a]									Fail

Notes: Results of the test of common true mean direction of McFadden and Lowes (1981) between locality mean directions in Central Greece.
[a]anomalously shallow inclination for the presumed eruption/deposition latitude.

Supplementary Figure Captions

Supplementary Figure 1. Acquisition of laboratory-induced gyroremanent magnetization (GRM) during alternating-field treatment of lacustrine marls. A) Demagnetization paths plotted on equal-area stereonets for three specimens are progressively deflected toward the Y=X line on the X-Y plane above peak fields of ~40 mT, reflecting the acquisition of a magnetization orthogonal to the applied transient field direction. B) Magnetization vs. applied field plots showing strong acquisition of magnetization above peak AF fields of ~85 mT for the same three specimens.

Supplementary Figure 2. Rock magnetic properties of representative Miocene/Pliocene lacustrine specimens. Linear acquisition (A, C) and gradient acquisition (B, D) plots show Gaussian component fits to room-temperature IRM acquisition data (squares). E, F) Room-temperature hysteresis curves after subtraction of a mass-specific paramagnetic component, showing typical open-loop forms.

Supplementary References

Atzemoglou, A., Kondopoulou, D., Papamarinopoulos, S., Dimitriadis, S., 1994. Paleomagnetic Evidence for Block Rotations in the Western Greek Rhodope. Geophys J Int 118, 221-230.

Avigad, D., Baer, G., Heimann, A., 1998. Block rotations and continental extension in the central Aegean Sea: palaeomagnetic and structural evidence from Tinos and Mykonos (Cyclades, Greece). Earth Planet Sc Lett 157, 23-40.

Bobier, C., 1968. Paleomagnetic study of some of the formations of volcanic Almopias Complex (Central Macedonia, Greece). Cr Acad Sci D Nat 267, 1091.

Broadley, L., Platzman, E., Platt, J., Papanikolaou, M., Matthews, S., 2006. Paleomagnetism and the tectonic evolution of the Ionian zone, northwestern Greece, in: Dilek, Y., Pavlides, S. (Eds.), Geol S Am S, pp. 137-155.

Deenen, M.J., Tol, J., Burylo, A.M., Doodeman, V.D., de Boer, A., Vincent, A., Guchelaar, H.J., Smits, P.H.M., Beijnen, J.H., Punt, C.J.A., Schellens, J.H.M., Cats, A., 2011. Relationship between Single Nucleotide Polymorphisms and Haplotypes in DPYD and Toxicity and Efficacy of Capecitabine in Advanced Colorectal Cancer. Clinical Cancer Research 17, 3455-3468.

Duermeijer, C.E., Krijgsman, W., Langereis, C.G., Meulenkamp, J.E., Triantaphyllou, M.V., Zachariasse, W.J., 1999. A Late Pleistocene clockwise rotation phase of Zakynthos (Greece) and implications for the evolution of the western Aegean arc. Earth Planet Sc Lett 173, 315-331.

Duermeijer, C.E., Krijgsman, W., Langereis, C.G., Ten Veen, J.H., 1998. Post-early Messinian counterclockwise rotations on Crete: implications for Late Miocene to Recent kinematics of the southern Hellenic arc. Tectonophysics 298, 177-189.

Duermeijer, C.E., Nyst, M., Meijer, P.T., Langereis, C.G., Spakman, W., 2000. Neogene evolution of the Aegean arc: paleomagnetic and geodetic evidence for a rapid and young rotation phase. Earth Planet Sc Lett 176, 509-525.

Edel, J., Kondopoulou, D., Pavlides, S., Westphal, M., 1991. Multiphase paleomagnetic evolution of the Chalkidiki ophiolitic belt, Greece, Geotectonic implications. Bull. of the Geol. Soc. of Greece 25, 370-392.

Edel, J.B., Kondopoulou, D., Pavlides, S., Westphal, M., 1992. Paleomagnetic Evidence for a Large Counterclockwise Rotation of Northern Greece Prior to the Tertiary Clockwise Rotation. Geodin Acta 5, 245-259.

Feinberg, H., Kondopoulou, D., Michard, A., Mountrakis, D., 1994. Paleomagnetism of some Northern Greece Ophiolites and Associated sediments. Bull Geol Soc Gr 30, 359-370.

Gürsoy, H., Piper, J., Tatar, O., 2003. Neotectonic deformation in the western sector of tectonic escape in Anatolia: palaeomagnetic study of the Afyon region, central Turkey. Tectonophysics 374, 57-79.

Haubold, H., Scholger, R., Kondopoulou, D., Mauritsch, H.J., 1997. New paleomagnetic results from the Aegean extensional province. Geol Mijnbouw 76, 45-55.

Horner, F., Freeman, R., 1983. Paleomagnetic Evidence from Pelagic Limestones for Clockwise Rotation of the Ionian Zone, Western Greece. Tectonophysics 98, 11-27.

Jordanova, N., Henry, B., Jordanova, D., Ivanov, Z., Dimov, D., Bergerat, F., 2001. Paleomagnetism in northwestern Bulgaria: geological implications of widespread remagnetization. Tectonophysics 343, 79-92.

Kaymakci, N., Aldanmaz, E., Langereis, C., Spell, T.L., Gurer, O.F., Zanetti, K.A., 2007. Late Miocene transcurrent tectonics in NW Turkey: evidence from palaeomagnetism and 40Ar–39Ar dating of alkaline volcanic rocks. Geol Mag 144, 379.

Kissel, C., Kondopoulou, D., Laj, C., Papadopoulos, P., 1986a. New Paleomagnetic Data from Oligocene Formations of Northern Aegea. Geophys Res Lett 13, 1039-1042.

Kissel, C., Laj, C., Mazaud, A., 1986b. First paleomagnetic results from Neocene Formations in Evia, Skyros and the Volos Region and the deformation of Central Aegea. Geophys Res Lett 13, 1446-1449.

Kissel, C., Laj, C., Muller, C., 1985. Tertiary geodynamical evolution of northwestern Greece - paleomagnetic results. Earth Planet Sc Lett 72, 190-204.

Kissel, C., Laj, C., Poisson, A., 1987. A paleomagnetic overview of the Tertiary geodynamical evolution of the Hellenic Arc. Terra Cognita 7, 108.

Kissel, C., Poisson, A., 1987. Étude paléomagnetique préliminaire des formations cénozoïques des Bey Daglari (Taurides occidentales, Turquie). Comptes rendus de l'Académie des sciences. Série 2, Mécanique, Physique, Chimie, Sciences de l'univers, Sciences de la Terre 304, 343-348.

Kondopoulou, D., 1982. Paleomagnétisme et déformations néogenes du Nord de la mer Egée. PhD Thesis, Université de Strasbourg.

Kondopoulou, D., 1994. Some constraints on the origin and timing of magnetization for Mio-Pliocene sediments from northern Greece. Bull. Geol. Soc. Greece 15, 53-66.

Kondopoulou, D., Caputo, R., 1997. Palaeomagnetic evidence for non-rotational deformation along the Nea Anchialos Fault System, Central Greece. Ann Geophys 40.

Kondopoulou, D., Lauer, J., 1984. Palaeomagnetic data from Tertiary units of the north Aegean zone. Geol Soc Spec Publ 17, 681-686.

Kondopoulou, D., Pavlides, S., 1990. Paleomagnetic and neotectonic evidence for different deformation patterns in the South Aegean volcanic arc: the case of Milos island. Proceedings of the IESCA, Izmir 1, 210-223.

Kondopoulou, D., Westphal, M., 1986. Paleomagnetism of the Tertiary Intrusives from Chalkidiki (Northern Greece). J Geophys-Z Geophys 59, 62-66.

Kondopoulou, D., Zananiri, I., Atzemoglou, A., Boidomatis, T., Michard, A., Feinberg, H.A., Pozzi, J.P., 2007. Neogene tectonic rotations in the vicinity of the north Aegean trough: new palaeomagnetic evidence from Athos and Samothraki (Greece). Bull Geol Soc Gr 40, 343-359.

Laj, C., Jamet, M., Sorel, D., Valente, J., 1982. First paleomagnetic results from Mio-Pliocene series of the Hellenic sedimentary arc. Tectonophysics 86, 45-67.

Lovlie, R., Stole, G., Spjeldnaes, N., 1989. Magnetic polarity stratigraphy of Pliocene-Pleistocene marine sediments from Rhodes, Eastern Mediterranean. Phys Earth Planet In 54, 340-352.

Marton, E., Drobne, K., Cosovic, V., Moro, A., 2003. Palaeomagnetic evidence for Tertiary counterclockwise rotation of Adria. Tectonophysics 377, 143-156.

Marton, E., Papanikolaou, D.J., Lekkas, E., 1990. Paleomagnetic Results from the Pindos, Paxos, and Ionian Zones of Greece. Phys Earth Planet In 62, 60-69.

Mattei, M., d'Agostino, N., Zananiri, I., Kondopoulou, D., Pavlides, S., Spatharas, V., 2004. Tectonic evolution of fault-bounded continental blocks: Comparison of paleomagnetic and GPS data in the Corinth and Megara basins (Greece). J Geophys Res-Sol Ea 109, B02106.

Mauritsch, H.J., Scholger, R., Bushati, S.L., Xhomo, A., 1996. Palaeomagnetic investigations in Northern Albania and their significance for the geodynamic evolution of the Adriatic-Aegean realm. Geol Soc Spec Publ 105, 265-275.

McFadden, P.L., Lowes, F.J., 1981. The Discrimination of Mean Directions Drawn from Fisher Distributions. Geophys J Roy Astr S 67, 19-33.

Morris, A., 1995. Rotational deformation during Palaeogene thrusting and basin closure in eastern central Greece: palaeomagnetic evidence from Mesozoic carbonates. Geophys J Int 121, 827-847.

Morris, A., 2000. Magnetic fabric and palaeomagnetic analyses of the Plio-Quaternary calc-alkaline series of Aegina Island, South Aegean volcanic arc, Greece. Earth Planet Sc Lett 176, 91-105.

Morris, A., Anderson, M., 1996. First palaeomagnetic results from the Cycladic Massif, Greece, and their implications for miocene extension directions and tectonic models in the Aegean. Earth Planet Sc Lett 142, 397-408.

Morris, A., Robertson, A., 1993. Miocene remagnetisation of carbonate platform and Antalya Complex units within the Isparta Angle, SW Turkey. Tectonophysics 220, 243-266.

Muttoni, G., Kent, D.V., Brack, P., Nicora, A., Balini, M., 1997. Middle Triassic magnetostratigraphy and biostratigraphy from the Dolomites and Greece. Earth Planet Sc Lett 146, 107-120.

Muttoni, G., Kent, D.V., Gaetani, M., 1995. Magnetostratigraphy of a Lower-Middle Triassic boundary section from Chios (Greece). Phys Earth Planet In 92, 245-260.

Piper, J.D.A., Tatar, O., Gursoy, H., Kocbulut, F., Mesci, B.L., 2006. Paleomagnetic analysis of neotectonic deformation in the Anatolian accretionary collage, Turkey, in: Dilek, Y., Pavlides, S. (Eds.), Geol S Am S, pp. 417-439.

Pucher, R., Bannert, D., Fromm, K., 1974. Paleomagnetism in Greece - indications for relative block movement. Tectonophysics 22, 31-39.

Sen, S., Valet, J.P., Ioakim, C., 1986. Magnetostratigraphy and Biostratigraphy of the Neogene Deposits of Kastellios Hill (Central Crete, Greece). Palaeogeogr Palaeocl 53, 321-334.

Spais, C., 1987. Palaeomagnetic and magnetic fabric investigations of Tertiary rocks from the Alexandroupolis area, NE Greece. PhD. Dissertation, University of Southampton.

Speranza, F., Islami, I., Kissel, C., Hyseni, A., 1995. Paleomagnetic evidence for Cenozoic clockwise rotation of the External Albanides. Earth Planet Sc Lett 129, 121-134.

Speranza, F., Kissel, C., Islami, I., Hyseni, A., Laj, C., 1992. First paleomagnetic evidence for rotation of the Ionian zone of Albania. Geophys Res Lett 19, 697-700.

Surmont, J., 1989. Paleomagnetism in the Internal Hellenides - superimposed magnetization analysis, using the remagnetization-circle method. Canadian Journal of Earth Sciences 26, 2479-2494.

Tozzi, M., Kissel, C., Funiciello, R., Laj, C., Parotto, M., 1988. A Clockwise Rotation of Southern Apulia. Geophys Res Lett 15, 681-684.

Turnell, H.B., 1988. Mesozoic evolution of Greek microplates from paleomagnetic measurements. Tectonophysics 155, 307-316.

van Hinsbergen, D., Dupontnivet, G., Nakov, R., Oud, K., Panaiotu, C., 2008. No significant post-Eocene rotation of the Moesian Platform and Rhodope (Bulgaria): Implications for the kinematic evolution of the Carpathian and Aegean arcs. Earth Planet Sc Lett 273, 345-358.

van Hinsbergen, D., Langereis, C., Meulenkamp, J., 2005. Revision of the timing, magnitude and distribution of Neogene rotations in the western Aegean region. Tectonophysics 396, 1-34.

van Hinsbergen, D.J.J., Dekkers, M.J., Bozkurt, E., Koopman, M., 2010a. Exhumation with a twist: Paleomagnetic constraints on the evolution of the Menderes metamorphic core complex, western Turkey. Tectonics 29.

van Hinsbergen, D.J.J., Dekkers, M.J., Koc, A., 2010b. Testing Miocene Remagnetization of Bey Daglari: Timing and Amount of Neogene Rotations in SW Turkey. Turkish Journal of Earth Sciences 19, 123-156.

Westphal, M., Kondopoulou, D., 1993. Paleomagnetism of Miocene volcanics from Lemnos island: implications for block rotations in the vicinity of the north Aegean Trough. Ann Tecton 7, 142-149.

Westphal, M., Kondopoulou, D., Pavlides, S., 1991. Paleomagnetism of late Tertiary and Plio-Pleistocene formations from Northern Greece. Bull Geol Soc Gr 25, 239-250.

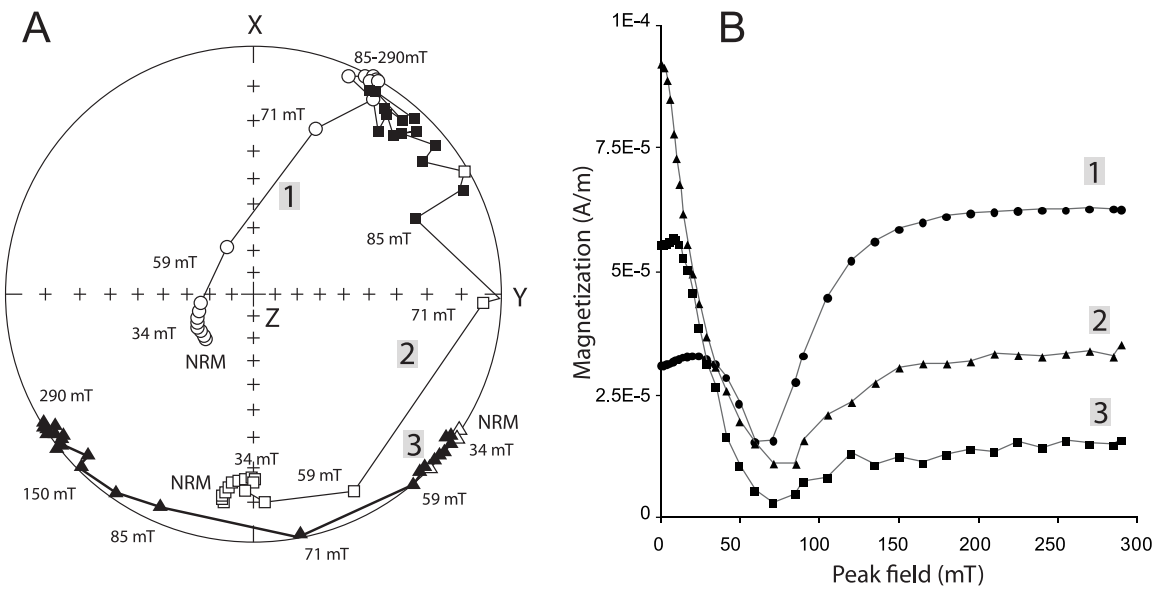

Supplementary Figure 1.

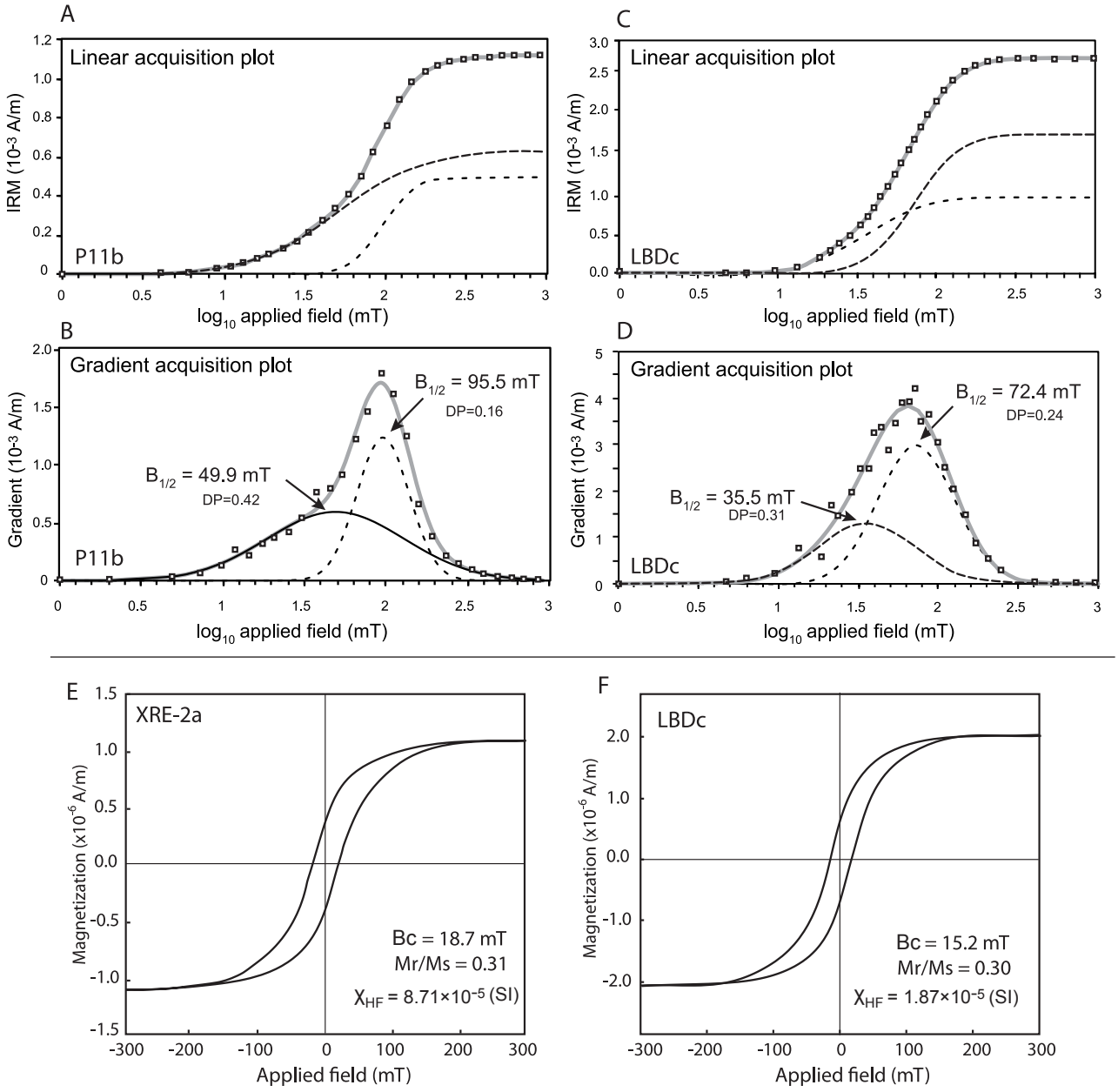

Supplementary Figure 2